Dietary methylmercury accumulates in pancreas and reduces basal insulin secretion in mice

INA MIDTTUN

MASTER THESIS IN HUMAN NUTRITION

INSTITUTE OF MEDICINE, UNIVERSITY OF BERGEN (UIB)

NATIONAL INSTITUTE OF NUTRITON AND SEAFOOD RESEARCH (NIFES)

MAY 2014

Dietary methylmercury accumulates in pancreas and reduces basal insulin secretion in mice

MASTER THESIS IN HUMAN NUTRITION

INA MIDTTUN

MAY 2014

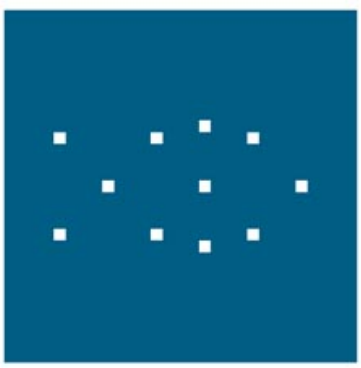

N I F E S

NASJONALT INSTITUTT
FOR ERNÆRINGS- OG
SJØMATFORSKNING

Acknowledgements

This master thesis was performed at the National Institute of Nutrition and Seafood research (NIFES) in Bergen, from autumn 2013 to spring 2014.

First, I would like to express my appreciation to my main supervisor Dr. Philos Lise Madsen for this great opportunity, and for valuable critiques and encouragement throughout this experience. I would also like to thank my co-supervisor Øyvind Lie.

I am particularly grateful for the assistance given by my co-supervisor Lene Secher Myrmel, your support and constructive suggestions during this process are very much appreciated. I also wish to acknowledge Ph. D Even Fjære for greatly appreciated contributions throughout this year. Thanks to Ph. D Ole Jacob Nøstebakken for guidance on aspects of toxicology.

I thank Aase Heltveit and Øyvind Reinshol for their excellent guidance in animal care. For technical assistance, I would like to thank Synnøve Winterthun, Hui-Shan Tung, Berit Solli and all the helpful technicians for their patient guidance.

To all my fellow students, thank you for the great company and great moments at the lunch table. I would also like to thank my family and friends. I thank Aina and Mette for genuine encouragement and support. I thank all my fantastic neighbors, and would like to express my great appreciation to Kristin and Kristine, for constant cheering and great friendship during this year.

Finally, I would like to express my deepest appreciation to my family, for being my inspiration and helping me keep in mind what is most important. I sincerely thank Cato Hakvåg for his love and support, and for believing that I can accomplish anything. Last but not least, I thank my wonderful daughter Pia for putting a smile on my face every day.

Ina Midttun

List of tables

List of figures

Appendix figures:

List of abbreviations

Acc1	*Acetyl-CoA carboxylase-1*
ADP	Adenosine Diphosphate
ANOVA	Analysis of variance
ATP	Adenosine Thriphosphate
AUC	Area under curve
BAT	Brown adipose tissue
Ccl1	*Chemokine ligand 1*
Cd68	*Cluster of differentiation 68*
cDNA	Complementary deoxyribonucleic acid
ELISA	Enzyme-linked immunsorbent assay
ETDA	Ethylenediaminetetraacetic acid
eWAT	Epididymal white adipose tissue
F4/80	*F4/80 antigen*
Fas	*Fatty acid synthase*
Foxo1	*Forkhead box protein O1*
Gl6	*Glucose 6 phospate*
GTT	Glucose tolerance test
iBAT	Interscapular brown adipose tissue
IRS	Insulin receptor substrate
ITT	Insulin tolerance test
iWAT	Inguinal white adipose tissue
MeHg	Methylmercury
MeHg-cys	Methylmecury-cysteine complex
NCD's	Non-communicable diseases

Pai	*Plasminogen activator inhibitor*
Pepck	*Phosphoenolpyruvate carboxykinase*
Ppara	*Peroxisome proliferator-activated receptor alpha*
Pparg	*Peroxisome proliferator-activated receptor gamma*
Ppargc1α	*PPARgamma Coactivator 1 alpha*
PTWI	*Provisonal tolerable weekly intake*
RT	Reverse transcription
RT-qPCR	Real time quantitative polymerase chain reaction
Scd1	*Stearoyl-CoA desaturase-1*
Srebp1-c	*Sterol regulatory element-binding protein 1-c*
Tbp	*TATA - binding protein*
Tnf	*Tumor necrosis factor*
WAT	White adipose tissue

Table of contents

Abstract

Lifestyle diseases like obesity and type 2 diabetes are highly prevalent worldwide, and represent a major public health concern. A potential link between lifestyle diseases and methylmercury exposure have been proposed in several studies. Methylmercury is an ubiquitous environmental contaminant emerging from both natural and anthropogenic sources. Methylmercury accumulates in the marine food chain and therefore represent a potential health risk for consumers. We aimed to investigate the potential role of methylmercury on obesity development and diabetes, evaluating dose response effects of methylmercury, and the effects on glucose tolerance and insulin sensitivity. In addition, we aimed to explore the accumulation of mercury in different tissues of the body. Obesity-prone C57BL/6 mice were exposed to an obesogenic high fat/high sucrose diet. Progressive concentrations of methylmercury-cysteine complex were added to the diets at 0.3 mg/kg, 1mg/kg, 3 mg/kg and 10 mg/kg. Our results demonstrated that chronic exposures to methylmercury did not induce obesity development: however, it attenuated obesity development and reduced basal insulin secretion due to the highest exposure (10 mg/kg). Further, we found a dose-dependent accumulation of mercury in several organs, with the highest levels accumulated in liver and pancreas.

1 Introduction

1.1 Non-communicable diseases (NCD's)

The global burden of lifestyle diseases is alarming. According to the World Health Organization (WHO), non-communicable diseases (NCD's), including cardiovascular disease, cancer, osteoporosis, chronic respiratory diseases, obesity and diabetes are currently the cause of 60% of all deaths (WHO, 2011). NCD's are largely preventable through the reduction of behavioral risk factors like physical inactivity and unhealthy diets, subsequently affecting development and progression of obesity and type 2 diabetes.

The increase in NCD's has been largely attributed energy imbalance, however, emerging evidence claim a more holistic view on this endemic (Chen et al., 2009; Grandjean et al., 2011). Findings from methylmercury (MeHg) exposed populations have given indications of an association with type 2 diabetes (Eto, 1997). However, studies in humans are limited and often contradictory and many questions remains unanswered (He et al., 2013; Mozaffarian et al., 2013). Still, both in-vitro studies and in-vivo studies using mouse models have linked MeHg to the development of type 2 diabetes (Chen et al., 2006b; Chen et al., 2006c). Given the tremendous burden of obesity and type 2 diabetes, clarifying the potential effects of MeHg would be a significant contribution to public health.

1.1.1 Overweight and obesity

Overweight and obesity are conditions of excessive fat accumulation that may have adverse effects on health (WHO, 2000). Overweight and obesity are commonly assessed using body mass index (BMI, kg/m^2), due to its strong correlation to body fat content. BMI measures should be in the range of 18.5 to 24.9 kg/m^2 for individuals to achieve optimal health. Obesity triggers adverse metabolic responses in blood pressure, triglycerides cholesterol, and insulin resistance thereby increasing the risk of coronary heart disease, ischemic stroke, type 2 diabetes mellitus etc. (WHO, 2011). Obesity is a complex disease that involves physiological, metabolic, social, cultural, educational, behavioral and genetic factors. Fundamentally, the development of overweight and obesity is caused by an imbalance between energy intake and expenditure (Bray, 2004). Modern society promotes an increase in energy consumption through a constant supply of cheap energy dense foods and persuasive food marketing (Lancet, 2011). Concomitantly, there is a reduction in physical activity due to a more sedentary environment,

ultimately leading to an excess of energy, which is stored as fat. This storage, through hyperplasia and/or hypertrophy of fat cells is essential in the pathology of obesity (Bray, 2004). White adipose tissue functions both as an energy storage and as an endocrine organ, and plays a pivotal role in the regulation of immune and inflammatory processes (Federico et al., 2010). The condition of obesity is characterized by low-grade systemic inflammation, caused by enlarged fat cells and the recruitment of macrophages. The secretion of adipokines, chemokines and cytokines (leptin, adiponectin, resistin, tumor necrosis factor alfa, interleukin etc.) from adipose tissue, have led to the discovery of several pathways linking adipose tissue metabolism and the immune system. Activation of the innate immune system, can in turn lead to impaired glucose tolerance, insulin resistance and type 2 diabetes.

1.1.2 Diabetes

The global obesity epidemic is accompanied by an increasing prevalence of type 2 diabetes (Kahn et al., 2014). Type 2 diabetes is characterized by elevated blood glucose and insulin resistance. Initially, insulin secretion increases but as the disease progresses, β-cell dysfunction and/or apoptosis occurs.

Glucose homeostasis is orchestrated by a number of factors, insulin being key due to its anabolic qualities distributing glucose throughout insulin sensitive tissues of the body. Insulin is synthesized, packaged and secreted from pancreatic β-cells. In the endocrine islets of Langerhans, insulin secretory β-cells are surrounded by α-cells, secreting glucagon. Insulin and glucagon counteract in keeping blood sugar within a fairly narrow range.

The regulation of blood glucose

Food intake leads to an increase of glucose and amino acids in the circulation. Elevated glucose levels increase glucose uptake through glucose transporters (GLUT2) into β-cells of the pancreas (Layden et al., 2010). Glycolysis transforms glucose to pyruvate, and the majority is transported to the mitochondria. The ATP/ADP ratio increase in line with glucose utilization through glycolysis, TCA cycle and oxidative phosphorylation (Rolo and Palmeira, 2006). This, in turn, stimulates ATP sensitive potassium (K^+) channels to close, causing depolarization of the β-cells through voltage-sensitive calcium (Ca^{2+}) channels (Layden et al., 2010). As the cells depolarize, membrane bound Ca^{2+} channels facilitate influx of Ca^{2+}. This intracellular calcium accumulation triggers the exocytosis of insulin vesicles and thereby β-cell insulin secretion.

Changes in ATP/ADP caused by mitochondrial dysfunction influences glucose stimulated insulin secretion (Lowell and Shulman, 2005).

The regulation of Ca^{2+} in pancreatic β-cells is mainly determined by the interplay between Ca^{2+} cell-entry, deposition of Ca^{2+} into intracellular compartments and elimination via microsomal Ca^{2+} pumps (Zhou et al., 1998). Inhibition of microsomal Ca^{2+} pumps causes depletion of intracellular calcium stores, which could increase intracellular free Ca^{2+}. Inhibitory actions on the complexes of the mitochondrial respiratory chain have been found to inhibit insulin output from pancreatic β-cells. Although insulin secretion is regulated by a number of factors separate from this pathway, it is evident that oxidative phosphorylation is essential in glucose stimulated insulin secretion (MacDonald and Fahien, 1990).

Insulin action

Once into the bloodstream, insulin exerts its biologic effects on various insulin-sensitive tissues as illustrated in fig.1-1 (Saltiel and Kahn, 2001). Activation of multiple signaling pathways influences a number of key regulatory transcription factors involved in metabolic processes. Skeletal muscle and liver are pivotal insulin-responsive organs responsible for the balance of glucose metabolism (Lowell and Shulman, 2005). Transition towards an insulin-resistant state in these organs are accountable for most of the perturbations of glucose homeostasis, seen in type 2 diabetes. In muscle, insulin promotes glucose uptake and storage of glycogen. Approximately 90% of insulin stimulated glucose uptake occurs in skeletal muscle (Leto and Saltiel, 2012). Although the insulin stimulated uptake in adipose tissue is markedly lower than muscle (10%) it is essential in regulating energy homeostasis. Adipose tissue responds to insulin by increasing glucose uptake and lipogenesis, successively storing energy as triglycerides. Under obese conditions, adipose tissue releases free fatty acids into the circulation in an uncontrolled manner. The increase in circulatory fatty acids potentially inhibits glucose uptake, glycogen synthesis and glucose oxidation, and increase hepatic glucose secretion. In addition, circulating cytokines secreted by adipose tissue might modulate insulin-responsiveness of skeletal muscle and liver, in which fatty acids and intracellular fatty acid metabolites are suggested to play a major role.

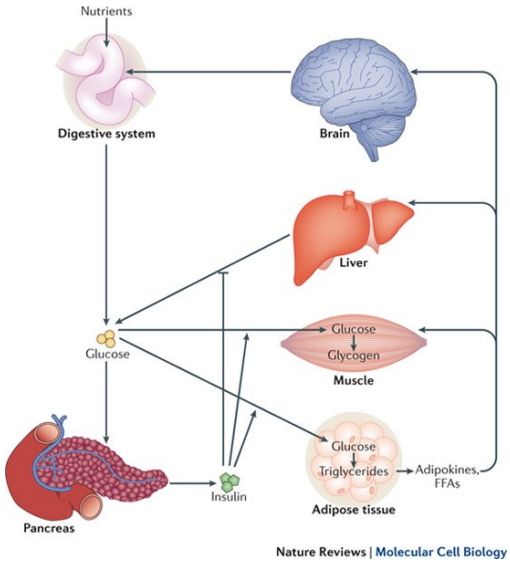

Figure 1-1. Energy homeostasis is dependent upon the crosstalk of multiple organs and tissues. Collectively, these organs respond to energy demand and availability through the release of hormones and metabolites. Defects in the response and miscommunication result in metabolic diseases, such as diabetes (Leto and Saltiel, 2012).

In the liver, insulin stimulates glycogen synthesis, lipogenesis and inhibits gluconeogenesis. Insulin inhibits several genes involved in gluconeogenesis, including *Foxo1*, *Pck1*, and *G6pc* (Saltiel and Kahn, 2001). In the presence of insulin, *Forkhead box protein-1* (*Foxo-1)* indirectly hinders gluconeogenesis through inhibitory actions on the transcription of *glucose-6-phophatase* (*G6pc*) and through the rate-limiting step, *phosphoenolpyruvate carboxykinase (Pck1)*(Quinn and Yeagley, 2005). Additionally, insulin influences the expression of transcription factors like sterol regulatory element-binding transcription factor *(Srebp1)*, which stimulate gluconeogenesis and lipogenic genes such as Acetyl-CoA carboxylase *(Acc1)* and fatty acid synthase (*Fas)* (Saltiel and Kahn, 2001).

In response to circulating insulin, glut 4 relocates to the cell membrane of fat and muscle to facilitate glucose entry into the cells (Leto and Saltiel, 2012). Insulin binds to its receptor (tyrosine kinase) at the cell surface, inducing phosphorylation of various insulin receptor substrates (IRS) (Leto and Saltiel, 2012). This family of adaptor proteins initiates the activation of other protein kinases and phosphatases, ultimately leading to insulin action. Metabolic processes are regulated through pathways that coordinate enzyme, activation/inactivation, protein synthesis, vesicle trafficking and gene expression.

In summary, insulin excise its profound anabolic abilities by stimulating the metabolic processes of energy storage and simultaneously inhibiting the processes that release energy into the bloodstream.

Counter regulatory mechanisms

Circulating glucose below a certain threshold stimulates counter regulatory mechanisms, mainly glucagon secretion from α-cells of the pancreas (Layden et al., 2010). Glucagon acts to increase hepatic glucose production, through induction of glycogen breakdown and/or *de novo* synthesis of glucose. The liver responds to glucose fluctuations, and regulates glucose release into the bloodstream. Additionally, circulating catecholamines, amino acids and hormones influence the insulin/glucagon ratio. The feedback loop regulating the glucose homeostasis is dependent on the continuous crosstalk between endocrine cells of the pancreas and insulin sensitive tissues (Kahn et al., 2014).

Metabolic disturbances

In the case of insulin resistance, β-cells sustain normal glucose tolerance by increasing the insulin output to compensate for the tissue insensitivity to the hormone (Ferrannini et al., 2005; Kahn et al., 2014). If β-cells fail to increase insulin secretion, an increase in plasma concentration of glucose follows.

Type 2 diabetics have exhibited both quantitative and qualitative perturbations of insulin levels (Rahier et al., 2008). Deterioration of β-cell function and reduction in β-cell mass inhibit the insulin capability of the pancreas (Kahn et al., 2014). A reduction in β-cell number is partly explained by glucolipotoxicity and amyloid deposition, triggering apoptosis through oxidative and endoplasmic reticulum stress (Jurgens et al., 2011). Amylin is normally co-secreted with insulin, when aggregated the formation of islet amyloid occurs. Glucolipotoxicity refers to the deleterious effects of increased levels of glucose and fatty acids on β-cells, increasing cellular lipids and eventually leading to apoptosis (Poitout et al., 2010). The combination of excessive levels of fatty acids and glucose, therefore leads to decreased insulin secretion, impaired insulin gene expression, and β-cell death by apoptosis.

Although insulin resistance and β-cell dysfunction is key in understanding the pathogenesis of type 2 diabetes, the combination of environmental and genetic factors also contribute to the disease. Genetic variation might predispose some individuals for the development of disorders related to the environment; diet and physical activity (McCarthy, 2010).

1.2 Methylmercury

Methylmercury (MeHg) is a highly toxic contaminant, arising from both natural and anthropogenic sources (ATSDR, 1999). Considerable emissions of mercury arise from natural sources, such as crust degassing, volcanoes, oceanic sediments and forest-fires and is further accompanied by man-made contributions like combustion of fossil fuels, chloralkali-manufacturing and coal mines (Morel et al., 1998).

Mercury exists in three basic forms: elemental (liquid), organic (mercury and carbon) and inorganic mercury (combined with chloride, sulfur, oxygen, also called salts)(ATSDR, 1999). Organic mercury compounds exist in a variety of formations; however, the most common organic mercury compound is MeHg. Once in the environment, inter-conversion between these compounds readily occurs. MeHg is of particular interest due to its ability to bio accumulate and bio magnify in the aquatic food chain.

The global cycle of Mercury

The chemical properties of mercury are of great importance when trying to understand the movement and deposition of the contaminant (Schaefer et al., 2011). Elemental mercury is a volatile compound (Hg^0), and the mercuric compound is highly reactive. The global cycle of mercury largely unfolds through reduction-oxidation reactions in the atmosphere and surface waters. Elemental mercury degasses from soil and surface waters, travels in the atmosphere and deposits onto land and surface waters (ATSDR, 1999). Further, the compound is absorbed into soil or particles in the sediment, and re-volatilization occurs. This process of emission-deposition and re-volatilization represents the challenge of trying to track the movement of Hg to its sources.

Methylation of elemental mercury

Methylation of mercury is a process where elemental mercury receives a methyl group from an organic compound (Morel et al., 1998). The first step in the methylation pathway is the conversion of elemental mercury (Hg^0), oxidizing to reactive species (Hg^2). The oxidation process occurs in air or aquatic environments (Mason et al., 1995). Whereas the oxidation occurs only to a small extent in fresh water systems, there is a substantial degree of oxidation in deep waters. Sulfate-reducing bacteria are responsible for the majority of mercury methylation in natural waters and sediments (Morel et al., 1998). Once methylated, the MeHg compounds may re-enter the atmosphere or bio- accumulate in the aquatic and terrestrial food

chain (ATSDR, 1999). The ability of MeHg to bio magnify in the marine food chain, creates a source for human consumption.

Human exposure to methylmercury

Humans are exposed to MeHg primarily through consumption of seafood (WHO, 2008). MeHg has a strong affinity for Thiols (Rooney, 2007), and is mostly bound to albumin, glutathione (GSH) or L-cysteine (Allen et al., 2001; Hirayama et al., 1991; Yasutake et al., 1997) . These complexes might predict body distribution of mercury, and possibly enhance mercury absorption and tissue accumulation (Hirayama, 1985). The MeHg-cysteine complex is structurally analogous to methionine, and thereby gains entry into the cells via amino acid carriers (Clarkson and Magos, 2006). MeHg from dietary sources are absorbed in the gastrointestinal tract and distributed throughout the body (Clarkson, 1972). Once arrived into the bloodstream, MeHg enters the red blood cells, extensively bound to hemoglobin (90%) (Kershaw et al., 1980). MeHg appears stable when consumed compared to other mercury species, and de-methylation towards less damaging inorganic mercury is slow. The major route of MeHg excretion occurs through bile and feces. Approximately 1% of the body burden is eliminated daily (Clarkson, 1988). MeHg slowly leaves the body, mostly as inorganic mercury in feces.

Upper Limits in Seafood

The concentrations of MeHg are minor in most fish species, but accumulation in the marine food chain contributes to higher levels in predatory fish, increasing with age and size (VKM, 2006). The upper limit of all mercury species in fish is set at 0.5 mg/kg (wet weight) (EFSA, 2012). In the case of some predatory fish (tuna, eel, halibut) the upper limit is set at 1.0 mg/kg. Despite potentially higher contents of mercury in these species, they represent a smaller proportion of the total fish intake. According to a report from the Norwegian Scientific Committee for Food Safety, lean fish contains approximately 0.05-0.08 Hg mg/kg, fatty fish contains approximately 0.01-0.1 mg/kg Hg and freshwater fish (pike, trout, perch) contains approximately 0.3-0.6 mg/kg (VKM, 2006). A report from Hardangerfjorden showed that the average mercury content of some deep-water species (Greenland halibut, tusk) was above 0.5 mg Hg/kg wet weight (Måge et al., 2011).

Tolerable weekly intake

Tolerably weekly intake of MeHg (expressed as mercury) is 1.3 µg/kg bodyweight/week (EFSA, 2012). This is equal to 0.09 mg/week for a person of average body weight (70 kg). The average seafood consumption among the adult population in Norway is 70 gram/day (VKM, 2006). Average intake of mercury from fish and seafood was 0.4 µg/kg body weight/week, among participants in the Fish and Game study. In 2006 the PTWI values for MeHg was slightly higher (1.6 µg/kg) and only 0.6% of the participants in the Fish and Game study exceeded this PTWI.

MeHg toxicity

Marine pollution by organomercurials first came to the worlds attention after a major accident in Japan in 1953. In a historical perspective, there has been several outbreaks of MeHg poisoning through fish-consumption (Eto, 1997; Tsubaki, 1967). The unfortunate outbreaks in Minamata bay (1953-1956) and Niigata city (1964-1965) was a consequence of industrial release. In 1973 a severe outbreak of MeHg poisoning occurred after consumption of MeHg treated grain (Bakir et al., 1973). MeHg poisoning display an array of adverse effects (neurological disturbances, impairment of speech, hearing, vision, sensory disturbances, tremor, mental disorders) (Ceccatelli et al., 2010) and in severe cases death has been the outcome. This comprehensive clinical picture was named Minamata disease.

The main toxicological organ for MeHg is the brain, and its detrimental effects as a neurotoxicant are well established (Ceccatelli, Dare et al. 2010). The evolving brain is the most susceptible to damage, and extreme fetal abnormalities were seen after the Minamata accident. MeHg readily cross the placental barrier and is excreted in breast milk subsequently reaching the fetus at its most fragile states.

Mechanism of methylmercury toxicity

A range of mechanisms have been proposed to underpin MeHg toxicity. Essential is the high affinity of MeHg for sulfhydryl and thiol groups (Clarkson, 1972). The formation of these complexes enables mercury to produce cell injury and apoptosis (Ceccatelli et al., 2010). Toxicity may be induced by oxidative stress via increased production of reactive oxygen species (ROS), or by a decrease in oxidative defense systems (Sarafian and Verity, 1991). Mercury has also been shown to induce mitochondrial dysfunction, which can cause disruption of Ca^{2+} homeostasis through an increase of intracellular Ca^{2+} or uncontrolled release of Ca^{2+} from the mitochondria due to oxidative stress (Atchison and Hare, 1994; Graff et al., 1997). Additionally,

it has been suggested that MeHg is capable of suppressing enzyme activity, interrupt microtubule formation, interfere in DNA and protein synthesis and trigger autoimmune responses (Ceccatelli et al., 2010).

1.3 Introduction to the experiment

There is great knowledge about the effects of methylmercury on neurological development and disorders (Ceccatelli et al., 2010), however, far less is known about the effects on type 2 diabetes. To our knowledge, the effects of MeHg on obesity development have not been studied. In the present investigation, obesity prone C57BL/6 mice were given a chronic dietary exposure to mehtylmercury-cysteine complex, implemented in obesogenic diets, during a 13 week feeding trial. The contamination pressures in the diets were:

- Non-supplemented low fat diet (LF)
- Non-supplemented high fat/high sucrose diet (HF/HS)
- HF/HS 0.3 mg/kg MeHg
- HF/HS 1 mg/kg MeHg
- HF/HS 3 mg/kg MeHg
- HF/HS 10 mg/kg MeHg

1.4 Aims

The current project aimed to explore the dose-response effects of methylmercury (MeHg) on diet induced obesity in mice, evaluating:

- The effects of MeHg on glucose tolerance and insulin sensitivity, including evaluation of glucose stimulated insulin secretion.
- The distribution and accumulation of MeHg in different organs.

2 Materials and Methods

2.1 Ethical aspect

This animal experiment is approved by the Norwegian animal research authority and the following procedures were performed in compliance with the current guidelines for the care and use of laboratory animals (National Research Counsil, 2011).

2.2 Experimental design

55 male C57BL/6JBomTac mice purchased from Taconic (Denmark), arrived at the animal facility at NIFES (Norwegian institute of nutrition and seafood research) at 7-8 weeks of age. Obesity prone C57BL/6J mice is appropriate due to its ability to develop obesity and type 2 diabetes (Surwit et al., 1995) Initially the animals were acclimatized, during this 5-day period, they were fed a chow diet and were given ad libitum access to water.

After acclimatization, the mice were weighed using a Mettler Toledo weight and scanned using a magnetic resonance instrument (Bruker Minispec LF50mq7.5) which provides a measurement of lean tissue, fat and fluid. The weights of the animals were ranging between 24.52±2.15 g, and they were divided into 6 groups (n=8) based on these recordings to achieve an equal baseline mean weight in each group.

A specific amount of food was weighed, registered, and fed to the animals three times a week (Monday, Wednesday, Friday) for 13 weeks. The remains were collected before feeding, and subsequently weighed and registered. Access to water was unlimited at all times. The animals were weighed once a week throughout the experiment. On the basis of these weekly recordings, development of the animals was tracked.

Housing

The mice were housed in individual plastic cages in a controlled environment (temperature 22±2 C° and humidity 50±5 %) with a 12-hour light/dark cycle. The cages were enriched with wooden chip bedding, a plastic house and nesting material. The animals were given clean cages and new bedding once every second week.

Preparation of diets

Experimental diets were prepared at NIFES based on a standard low fat (LF) and high fat/high sucrose (HF/HS) setup. Appendix I: Table A.1 and A.2 display dietary ingredients of the different diets as well as the suppliers. The different components were weighed in using a laboratory weight (Mettler Toledo PG42002-S/PH), and mixed in a blender (Crypto Peerless EF20 blender).

A stock solution of MeHgCl was made by dissolving 1 g MeHgCl (Sigma Aldrich) in 50 ml ethanol. L-cysteine was prepared by dissolving 7.5 g of L-cysteine in 1 litre of distilled water. This solution was prepared fresh prior to every batch of feed. An equimolar mixture was made by combining these solutions, and the mixture was added to the diets. For the control diets an 1:1 solution of ethanol and water was added. Aliquots of the methylmercury-cysteine (MeHg-Cys) solution was added to the feed mixture in combination with 30 percent water, according to Appendix I: Table A.3. The supplementation of MeHg-cysteine was performed by trained personnel. Color was added to ensure separation of the different doses, throughout the experiment. Finally, the feed mixture was sculptured in a pellet-mold, frozen and subsequently dehydrated using a vacuum freeze-dryer (Christ, Lyo chamber guard). The lipophilization process occurs through, a direct conversion from ice to vapor. Feed was contained at -20 C° to maintain quality of the diets.

Each group received different diets; HF/HS diet supplemented with increasing concentrations of MeHg (0.3 mg/kg, 1 mg/kg, 3 mg/kg, 10 mg/kg). A non-supplemented low fat diet and high fat/high sucrose diet were used as references (Betty L. Black, 1998; Petro et al., 2004). The macronutrient composition of the background diets are shown in fig. 2.1. To verify dietary contents, a random selection of feed was analyzed. The mercury content was on average 0.54, 0.83, 2.4, 8.29 mg/kg. The total contents of the diets are provided in Appendix I: Table A.1.

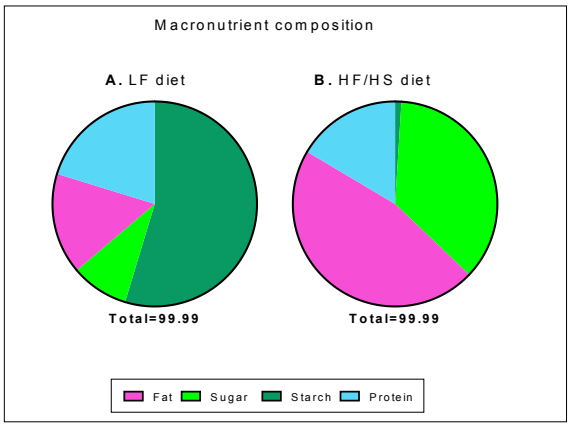

Figure 2-1. Distribution of fat, sugar, starch and protein in the experimental diets. A: Low fat control diet. B: Non-supplemented HF/HS was the control diet and the background diet for MeHg supplementation.

Food-Intake and Weight Development

The mice participated in a 13-week feeding-trial. They were fed three times a week (Monday, Wednesday, and Friday) for 13 weeks. At feeding, the amount of pellets and residues were registered by weighing. Based on total body weight gain and food intake, feed efficiency (the amount of calories necessary to produce 1 gram of weight gain) was calculated, using the formula below;

$$Feed\ efficiency = (\text{Body weight gain (g)})/(\text{Food intake (Kcal)})$$

Body scan

Mice were subjected to a non-invasive examination; magnetic resonance scan to reveal body composition (body weight, fat mass, lean mass and water content). Scanning was performed at baseline and after 6 and 9 weeks of feeding.

Collection of feces

Feces was collected after 3 and 9 weeks of feeding. The mice were transferred to clean cages with paper bedding for a 7 days period, food intake and weights were recorded, and feces was collected at the end of the period. Samples were weighed, stored in small containers at -20°C awaiting further analysis. Subsequently, the total fat content of feces was measured and apparent fat digestibility (AFD) was calculated using the formula below:

$$AFD = ([\text{Fat consumption}] - [\text{Fecal excretion}])/([\text{Fat consumption}]) \times 100$$

Insulin Tolerance test

At the end of the exposure period (11 weeks) an insulin tolerance test (ITT) was performed. The animals were moved to small cages. Baseline blood glucose was measured in fed state and an intraperitoneal injection of insulin was administered at a dose of 1U/kg lean bodyweight. Blood glucose levels were measured at 15, 30, 45 and 60 minutes. Further, the homeostasis model assessment was used to evaluate insulin resistance (HOMA-IR). Fasting insulin and glucose levels were used in order to calculate HOMA-IR by the following formula:

$$\text{HOMA} - \text{IR} = [\text{Fasting glucose (mmol/L)}] \times [\text{Fasting insulin (mU/L)}] \ /22.5$$

Oral Glucose Tolerance test

An Oral Glucose tolerance test (OGTT) was performed after 10 weeks of feeding (Andrikopoulos et al., 2008). The individual glucose load was determined based on the lean mass of each animal. Initially, the mice were weighed and placed into small cages, with ad-libitum access to water. After 6 hours of fasting they were weighed again, baseline was established and they were given an oral dose of 3 mg/g lean bodyweight glucose solution (200 mg/ml glucose injection fluid) using an oral gavage syringe. Blood glucose was measured at 15, 30, 60 and 120 minutes using a glucometer (Contour next blood glucose meter). Blood samples were collected in EDTA containing tubes, centrifuged at 2500g at 4°C for 10 minutes. Plasma was transferred to new tubes and stored at -80 C°. Subsequently, insulin levels in plasma were quantified using enzyme-linked immunosorbent assay (ELISA) kit for mouse (DRG Instruments, GmbH, Germany). Analysis was performed according to manufacturers manual (DRG Instruments, GmbH, Germany) and the ELISA kit reagents are listed in Appendix II: Table A4.

2.3 Sampling

After 13 weeks of feeding the experiment was terminated. Before euthanization, the mice were randomly fed, given ad libitum access to water and weighed. The termination process was performed by trained personnel. The animals were anaesthetized with Isoflurane (Isoba-vet, Schering Plough, Denmark) using an anesthesia unit (Univentor 400 Anesthesia Unit (Univentor Limited, Sweden) and blood collected by cardiac puncture. The sternum was opened using a scalp and a syringe was placed gently into the heart to collect blood samples. The samples were immediately collected in EDTA anticoagulant tubes, centrifuged at 2500g in 4

C° for 5 minutes, separating red blood cells and plasma. One mice from the non-supplemented HF/HS control group, unexpectedly deceased during the experiment.

Tissue collection and storage

Liver, kidneys, spleen, brain, heart, tibialis muscle and pancreas were collected. Additionally four fat depots were excised; visceral white adipose tissue depots; epididymal (eWAT) and retroperitoneal (rWAT), the subcutaneous white adipose tissue depot; inguinal (iWAT) and the brown adipose tissue depot; intrascapular (iBAT). Organs were dissected out, weighed and flash-frozen in liquid nitrogen. Samples were kept on dry ice during the sampling process and stored at -80 C° for further analysis.

2.4 Quantitative Real Time Polymerase Chain Reaction

Quantitative real time polymerase chain reaction (qPCR) was performed to quantify the relative gene expression level in mouse liver. The expression was normalized to a housekeeping-gene (TATA binding protein) known to transcribe at a relatively constant level.

Tissue homogenization and RNA extraction

Principle: The tissues were homogenized in Trizol. Trizol contains phenol and guanidine salts that takes part in solving biological material and denaturing protein. Chloroform separates RNA from the proteins and deoxyribonucleic acid (DNA). RNA is precipitated from the water phase by adding Isopropanol. The RNA is solved in ddH_2O.

Procedure: Before starting the procedure all surfaces and equipment were cleaned with RNase Zap and tissue samples transferred to 1.5 ml RNAse free tubes after thawing on ice. 3 Zirconium beeds and 1 ml Trizol was added into the tubes, followed by homogenization at 6000 rpm, 3x15 sec. The tissue samples were centrifuged for 10 minutes at 12 000g 4 °C, and the homogenate transferred to a second tube and incubated for 5 minutes at room temperature. The homogenate was centrifuged for 10 min at 12 00g. 200µl chloroform was added, and the tubes were manually shaken for 15 sec. The samples were incubated at room temperature for 2 minutes and centrifuged for 15 min at 12 000g 4 °C. The aqueous phase was transferred to a clean tube, 500 µl Isopropanol was added and the tubes were gently mixed. The samples were incubated for 10 min at room temperature and 10 min at 4 °C, followed by 30 min of centrifuge at 12 000*g. The supernatant was removed with vacuum suction, 1 ml cold 75%ETOH was added and the tubes were whirled and centrifuged for 5 minutes at 10 000*g. This step was repeated one time. Then absolute EtoH was added, whirled and centrifuged at 13000*g for 5 minutes. The supernatant was removed to allow the RNA pellet to dry. The pellets were dissolved in 50-200 µl of ddH_2O, depending on the size of the pellets. RNA concentrations were measured with a Nano Drop. A_{260}/A_{280} ratio between ≥1.8-2.1 is preferable. <1.80 might indicate Phenol, DNA or protein remnants in the sample. Chemicals and reagents used during this procedure are listed in Appendix III: Table A5.

RNA Precipitation

Principle: Precipitation is a process used to improve the quality of the sample by altering the A_{260}/A_{230} ratio, which is an indicator of the purity of the sample. Remaining residues of salt (or other inhibiting factors) might lower the ratio that preferably locates at >1.8.

Procedure: The samples were thawed on ice. 0.1 volume 3 Molar NaAc pH 5.2 and 2.5 volume of absolute EtOH was added. The samples were incubated for 1 hour at -80°C. After incubation the samples were centrifuged at 12 000g for 15 minutes at 4°C. The supernatant was carefully removed with vacuum suction, 1 ml 75% EtOH was added and the samples whirled. Centrifuged at 12000g for 5 minutes at 4°C, remaining liquid was removed again, and 30-200µl DEPC H_20 was added, depending on the size of the pellets. Chemicals and reagents are listed in Appendix III: Table A6.

RNA Quality

Principle: RNA 6000 Nano is a miniature edition of the RNA electrophoresis method. The RNA is separated by size in the channel system of the chip. The migration of RNA is detected, by which RNA integrity number (RIN) can be calculated.

Procedure: 12 representative samples were thawed on ice. The RNA6000 Nano kit was brought to room temperature. The light sensitive RNA Nano Dye was kept in a dark container. 550 µl of gel matrix was filtered and centrifuged at 1500g for 10 minutes, and a 32µl aliquot was prepared. The Gel Dye mix was whirled and spinned down. 0.5 µl RNA Nano dye was added to the filtered gel matrix. The samples were whirled and centrifuged at 13 000g for 10 minutes. The RNA concentration was adjusted to 100-500µg/µl. The bio analyzer was prepared by decontaminating the electrodes using a wash-chip filled with water and RNaseZap. Before loading the samples, the Nano chip was placed in a priming station. The microchip contains 16 wells were sample and reagents are loaded in a specific order. 9µl gel dye-mixture was added into three of the wells, the priming station closed, incubated and then opened before the complete loading was performed. Further, 5 µl of marker was added to all the wells (except those containing gel). 1µl ladder was added into one single well. The RNA samples incubated for 2 minutes at 70°C and 1µl RNA sample was added into 12 wells. The chip was whirled for 1 minute at 2400rpm (IKA vortex mixer), and analyzed on the Bio analyzer within 5 minutes. See Appendix III: Table. A7 for a detailed list of chemicals and reagents and figure. A.1 for the RIN numbers obtained from the bio analyzer.

Reverse transcriptase reaction

Principle: RNA is transcribed to complementary DNA (cDNA) by the enzyme reverse transcriptase. cDNA is a more stable compound and can be interpreted by the qPCR.

Procedure: The samples were thawed on ice, and kept on ice for the entire procedure. The concentration of RNA in the samples were adjusted on the nano drop until they had a concentration of 50ng/µl ±5%. 3 µl of RNA from all the samples was added into single tubes. An aliquot of 90µl was made, and adjusted to 100ng/µl±5% on the nano drop. Based on the RNA mixture the standard curve was set up with concentrations from 100- 50- 25- 12,5- 6,25- 3,125 ng/µl.

Reverse transcriptase reagents were thawed on ice, and enzymes kept on a freezing block in a clean room. A 96 well RT plate was prepared as described in Appendix III: Table A8. 40 µl reverse transcriptase mix was added into all the wells. 10 µl RNA/well was added to the RT plate (Standard curve triplicates and sample duplicates). As well as two negative controls; Non-amplification control (nac), containing no enzyme and Non-template control (ntc) containing no RNA. The cDNA plate was centrifuged for 1 minute at 50g and placed in the PCR machine. The PCR machine was set on a specific temperature program (10 minutes for 25C°, 60 minutes for 48C°, 5 minutes for 95C°) and the cDNA plate was stored at -20 C° until Real time qPCR analysis.

Real Time PCR

Principle: The Real time PCR method is based on the amplification of small DNA sequences coding for the gene of interest. The amplification of DNA is an exponential process detectable by fluorescence.

Procedure: The cDNA plate was thawed on ice and diluted by adding 50 µl ddH20. Centrifuged at 1000g for 1 minute and whirled at 1300 rpm for 3 minutes. Reagents were thawed on ice at the RNA-free lab. The real time reaction mix was made by mixing the reagents in Appendix III: Table. A8.

Using a robot (Biome 3000 Laboratory Automation 31 Workstation, Beckman Coulter, USA). 8µl of reaction mix and 2µl cDNA was added to a 384 well real-time PCR plate. An optical adhesive cover was placed on top of the plate and it was centrifuged at 1500g for 2 minutes Finally, the cDNA plate was placed in a Light cycler 480 and analyzed by a real-time PCR program according to manufacturers manual. Primers are shown in Appendix III: Table A9.

2.5 DMA80 – Direct Mercury Analyzer

Principle: The sample is dried through several steps of combustion, chemically decomposing the analyte from the sample trough thermolysis. A constant oxygen flow carries the thermolytic products through a catalyst bed, trapping interferences. Remaining mercury species are reduced to elemental Hg and trapped in a gold amalgamator. The amalgamator is reheated, releasing mercury vapor into a single beam of light at a specific wavelength. The amount of mercury in the sample is proportional to the absorbance at 254 nm, read by atomic absorbance spectrophotometry.

Procedure: Total Hg concentrations were measured in organs and feces from each individual mouse using atomic absorption spectrophotometry (Direct mercury analyzer, DMA80). The samples were weighed into a nickel boat and positioned in the auto sampler. Sample preparations were not required, and results were obtained directly from a software.

Certified Reference Material (CRM) for trace metals were included in duplicates, twice at every run to assess the accuracy/quality of the analysis. Oyster tissue (37.1 ng/g ±7.40) and TORT-3 Shellfish tissue (292±58µg/kg) were used, due to correspondent concentration levels compared to the respective samples. The mean values obtained from certified reference material were ranging within 2 standard deviations. Despite one DMA80 run, were one of the certified reference materials were within 3 standard deviations. Blanks were regularly distributed throughout every run, to clean the instrument and to exlude memory effect from one sample to another.

2.6 Histology

In order to investigate the morphology of the insulin secreting organ, pancreatic tissue was zinc-formalin fixed, paraffin embedded pancreas specimens were cut into 5 um sections and stained. A random selection of tissue from each group was stained with hematoxilin/eosin, and Hoechst 33258. The islet mass and cell nuclei were assessed, respectively. Reagents and solutions are listed in Appendix IV: Table. A10.

Fixation with zinc formalin fixative

The fixation medium preserves the structure and morphology of the tissue, by inhibiting enzymatic autolysis and degradation due to bacteria. A small section of pancreatic tissue was placed in a (histology) cassette and immediately fixated in zinc formalin fixative, diluted in 0.1 M Phosphate buffer (PB). The next morning the cassettes were washed once in PB and contained in PB until dehydration.

Dehydration and paraffin embedding

After preservation, the tissues were dehydrated in a progressive series of ethanol dilutions, gradually removing fixation medium and water. The time schedule is shown in Appendix IV: Table. A11. When dehydrated, tissue was transferred to xylene, and further infiltrated in liquid paraffin. Finally, tissues were embedded in paraffin to form blocks, using a paraffin embedding center (Microtom international, Germany).

Sectioning with microtome and staining

The paraffin blocks with tissue were positioned on the microtome (Leica RM 2165) and cut in sections of 5 μm. Sections were transferred to heated water (33-35°C) (Slide warmer SW 85). A small amount of Methanol was added to the water to help stretch the tissue. Tissues were collected with a microscope slide and left to dry over the weekend. Further, the tissue was stained in order to visualize the cell structures in a microscope. Prior to staining the slides were heated at 57°C for 60 minutes in a heating cabinet**.** Twenty random sections of pancreas from HF/HS control and all treatment groups were rehydrated, stained and dehydrated following the procedure in Appendix IV: Table A12. Hematoxilin and eosin was applied to stain the nucleus and the cytoplasm of the cell, respectively. After staining the slides were mounted with xylene based glue, a cover glass and left to dry. Additionally, twenty random sections of pancreas from HF/HS control and 10 mg/kg was rehydrated and stained following the procedure in Appendix

IV: Table A13. Sections were stained with a fluorescent dye (Hoechst 33258) to identify nuclei. Tissue slides were mounted with fluorescent mounting medium, a cover glass and left to dry.

Microscopy and image analysis

The pancreas sections from the control group (HF/HS) and the 10 mg/kg MeHg-group were compared using a binocular microscope (Olympus BX 51 binocular microscope). Twenty sections stained with hematoxilin/eosin were assessed in the microscope. Four representative sections of HF/HS and 3 sections of 10 mg/kg group was used to measure the volume of Langerhans islets of the pancreatic section. Image J, measurement tool was used to outline the islets, and total area in order to calculate the islet mass of the sections. Finally, twenty sections stained with Hoechst 33258 were assessed in the microscope to identify nuclei.

2.7 Statistical analysis

Statistical methods were used in the search for statistically significant differences between the different groups in the experiment. All data was continuously entered into excel to be able to follow development in the experiment. Statistics were performed using Graphpad Prism 5.0. D'Agostino Pearson omnibus test was used to assess normality of distributions of each treatment. Outliers were detected using Grubb's test for outliers, and significant outliers were removed. Data was analyzed by One way analysis of variance (ANOVA) followed by Dunnet's multiple comparison test (Unless otherwise stated). All treatment groups were compared to high fat/high sucrose control. Low fat-control was included as a reference. Differences between groups were considered significant when $p<0.05$. Data were presented as mean ±SEM.

STATISTICA: Repeated measurements ANOVA was performed on data from the curves of body weight development, ITT, OGTT and GSIS. All data were tested for normality of distributions (PP plot) and homogeneity of variance (Levenes test).

3 Results

3.1 Body weight development and feed intake

To investigate the effect of methylmercury (MeHg) on the development of obesity and diabetes, a 13 week feeding experiment was performed. Obesity-prone C57BL/6 mice were fed a high fat/high sucrose diet, spiked with increasing amounts of methyl mercury. A non-supplemented low fat diet and a high fat/high sucrose diet was included as reference. The development in body weight and feed intake are presented in fig. 3-1.

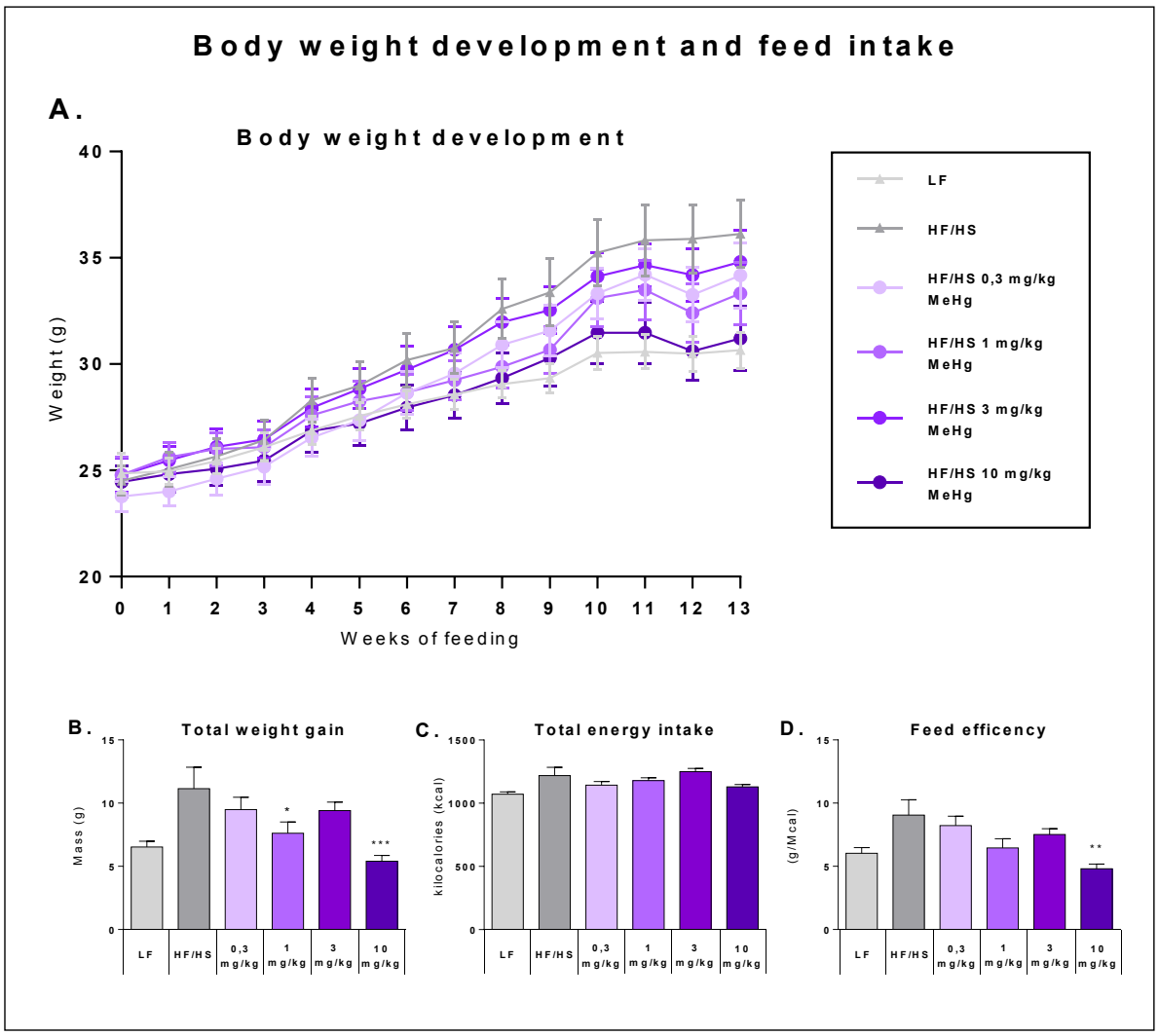

Figure 3-1. Body weight gain and feed intake in the different experimental groups (n=8). A: Weekly body weight (g) recording in all treatment groups during 13 weeks of feeding. Repeated measurements ANOVA not significant. B: Total weight gain (g). C: Total energy intake (Kcal) during feeding trial. D: Feed efficiency. All values expressed as mean ± SEM. * Refer to significant differences from non-supplemented high fat/high sucrose group according to posthoc, Dunnet's test (*P<0.05, **P<0.005, ***P<0.0005*).

MeHg did not significantly increase body weight development or weight gain (Fig. 3-1 A). As expected, mice fed the low fat reference diet, gained less weight than all HF/HS groups. In fact, the non-supplemented HF/HS group gained the most weight, considering all groups. Consequently making the MeHg exposed groups, randomly distributed between the LF and the HF/HS diets. Conversely, the total weight gain was significantly lower in 1 mg/kg and 10 mg/kg MeHg fed mice compared to HF/HS group (Fig. 3-1 B).

To exclude the possibility that the modest weight gain in 1 mg/kg and 10 mg/kg groups were explained by a reduction in total energy intake, total caloric intake was measured and feed efficiency and was calculated (Fig. 3-1 C and D). All groups displayed a similar total energy intake, despite contamination pressure (Fig. 3-1 B). Thus implying an increase in MeHg had no effect on the energy intake. The amount of calories necessary to produce 1 gram of weight gain was calculated, to evaluate if MeHg concentrations had an impact on energy efficiency. The feed efficiency was significantly lower in the 10 mg/kg MeHg fed mice compared with the non-supplemented HF/HS group (Fig. 3-1 D) and thereby had twice the energy cost to establish the same weight gain as opposed to the HF/HS group.

3.2 Whole body analysis

To gain further insight on whether the restricted weight gain in mice at different exposure regimens was due to changes in fat mass or lean mass, an MRI-scan was performed. Data from the scan are shown in fig. 3-2.

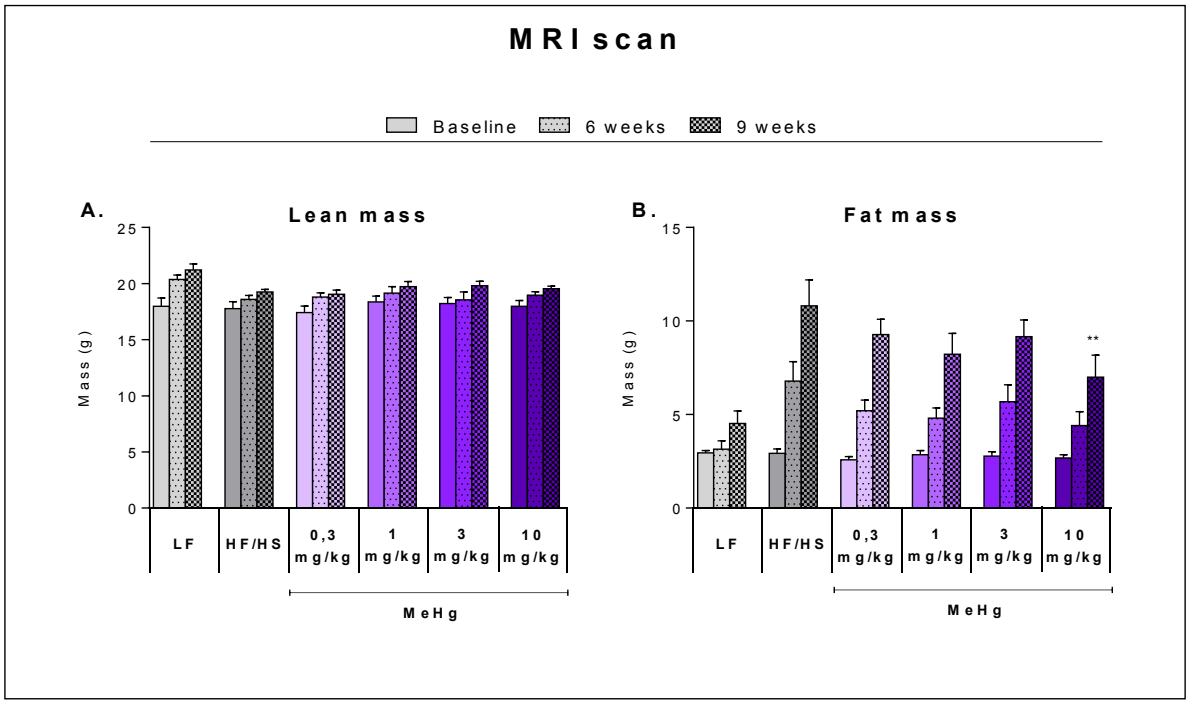

Figure 3-2. Body composition, distinguished between fat and lean mass (g) at baseline, 6 and 9 weeks of feeding. A: Lean mass (g) B: Fat mass (g) One-way Anova was performed to assess differences within each group. Baseline of HF/HS was compared to baseline of all treatment groups, and likewise for 6 and 9 weeks. All values expressed as mean ± SEM. * Refer to significant differences from non-supplemented high fat/high sucrose group according to posthoc. Dunnet's test (*P<0.05, **P<0.005).

MeHg exposure did not significantly alter the lean mass of the animals, according to the MRI-scan (Fig. 3-2 A). Comparison within each individual group displayed no significant differences in the lean mass of the animals (Fig. 3-2 A). Moreover, no differences emerged when comparing any of the groups exposed to MeHg, compared to HF/HS control. Indicating that changes in body weight probably occurred due to a variation of fat mass.

Comparison within each individual group showed no significant differences in the fat mass of the animals. Concurrent with the limited weight gain in mice exposed to 10 mg/kg, they exhibited a significant reduction in fat mass after 9 weeks of feeding (Fig. 3-2 B).

3.3 Fat depot masses

To explore the effects of the experimental diets on the adipose tissues of the mice, four different fat depots were dissected out and weighed. The weight of white adipose tissue depots; visceral, subcutaneous and abdominal, as well as the intrascapular brown adipose tissue, are shown in fig. 3-3, respectively.

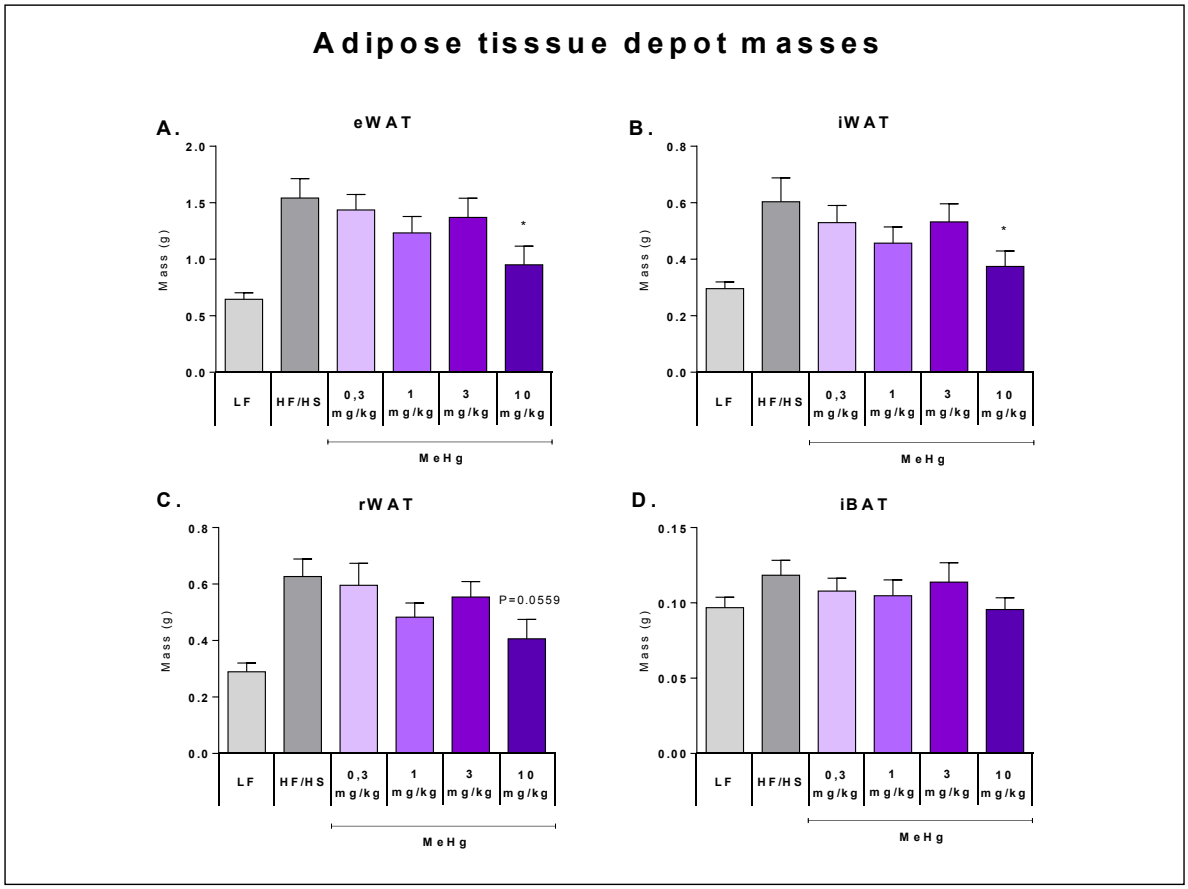

Figure 3-3. The weight of four different adipose tissue depots (g). A: Epididymal adipose tissue B: Inguinal white adipose tissue C: Retroperitoneal adipose tissue D: Intrascapular brown adipose tissue. All values expressed as mean ± SEM. * Refer to significant differences from non-supplemented high fat/high sucrose group according to posthoc. Dunnet's test (*P<0.05). P for trend (P=0.05-0.1).

Mice fed the 10 mg/kg MeHg diet, exhibited a significant decrease in visceral fat, compared to the HF/HS control diet (Fig. 3-3 A). Equally, the subcutaneous fat pad was significantly decreased in 10 mg/kg, compared to that of HF/HS control (Fig. 3-3 B). Further, the 10 mg/kg MeHg group displayed a trend towards reduced abdominal fat depots (Fig 3-3 C), whereas no significant alterations of fat mass was evident in brown adipose tissue (Fig 3-3 C-D). Besides mice fed the highest exposure regimen, no significant changes were seen in fat depot masses.

3.4 Apparent fat digestibility

Further, feed digestibility was calculated, to investigate whether the observed differences in energy efficiency originated from differences in energy absorption. Feed intake and fecal excretion of mice were recorded for one week. Subsequently, the total fat content was measured in feces and apparent fat digestibility (AFD) was calculated. Apparent digestibility is presented in fig. 3-4.

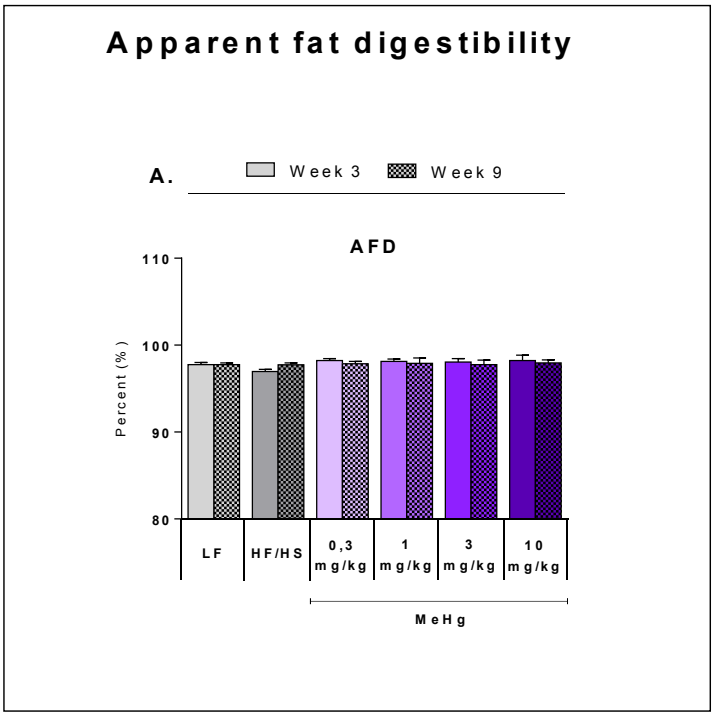

Figure 3-4. Apparant fat digestibilty. A: AFD (%) after 3 weeks and 9 weeks of MeHg exposure. All values expressed as mean ± SEM.

MeHg exposure did not significantly alter the fat digestion in any of the groups (Fig. 3-4 A). Fat digestion from the third week of the experiment, was comparable to the digestion after nine weeks, an indication that excretion remained stable throughout the experiment.

3.5 Effects of methylmercury on glucose tolerance in mice

In order to explore the effect of MeHg on glucose tolerance, an oral glucose tolerance test was performed. Mice were fasted for six hours and given an oral dose of glucose based on their body weights. Blood glucose was measured, followed by glucose measurements as 15, 30, 60 and 120 minutes. Blood glucose responses during the test are shown in fig. 3-5.

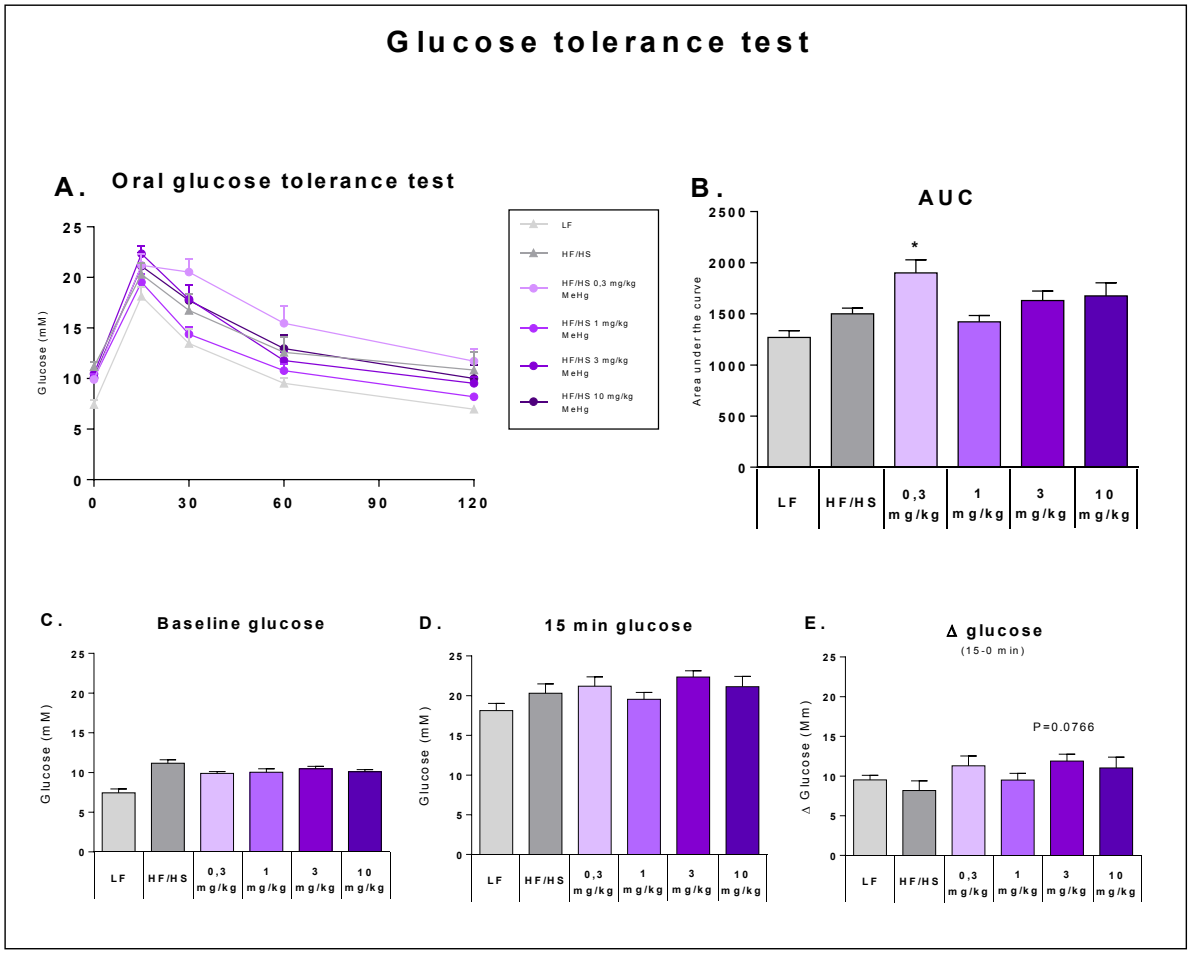

Figure 3-5. OGTT performed after 10 weeks of methyl mercury exposure. A: Levels of blood glucose at baseline, 15 min, 30 min, 60 min, 120 min after glucose administration, in all groups. Repeated measurements ANOVA not significant. B: Area under the curve. C: Baseline levels of blood glucose. D: Glucose levels 15 minutes after glucose administration. E: Delta blood glucose; (15-0 min). All values expressed as mean ± SEM. * Refer to significant differences from non-supplemented high fat/high sucrose group according to posthoc Dunnet's test (*P<0.05). P refer to a trend (P=0.05-0.1).

Results from the oral glucose tolerance test showed that MeHg was associated with a reduction in glucose tolerance in the 0.3 mg/kg MeHg group, indicated by significantly elevated glucose area under the curve, compared to the control group (Fig 3-5 B). When assessing the OGTT

curve, mice fed 0.3 mg/kg MeHg had a sustained peak in blood glucose and a reduced glucose disposal from the blood, although not significant. All groups exhibited a normal response, with a peak in blood glucose 15 minutes after glucose administration followed by normalization of glucose levels after two hours, but no significant differences were observed (Fig 3-5 A).

Fasted plasma levels of glucose were similar between the experimental groups (Fig. 3-5 C). 15 minutes after glucose administration, all groups displayed a similar response with elevated levels of glucose, as expected (Fig. 3-5 D). Further, when assessing the pancreatic response to a glucose load (15-0 min), no significant alterations were observed between exposure regimens (Fig. 3-5 E). Yet, a trend towards higher glucose levels were seen in mice exposed to 3 mg/kg MeHg ($P=0.0766$). Repeated measurements ANOVA detected no significant differences between diets on the glucose tolerance of the mice (Fig 3-5 A).

3.6 Effects of methylmercury on glucose stimulated insulin secretion in mice

To explore the potential effects of MeHg on glucose stimulated insulin secretion (GSIS), blood samples were collected during the OGTT at baseline and after 15 and 30 minutes. Plasma from these samples were analyzed using a mouse ELISA kit as previously described. The Insulin levels during the OGTT are presented in fig. 3-6.

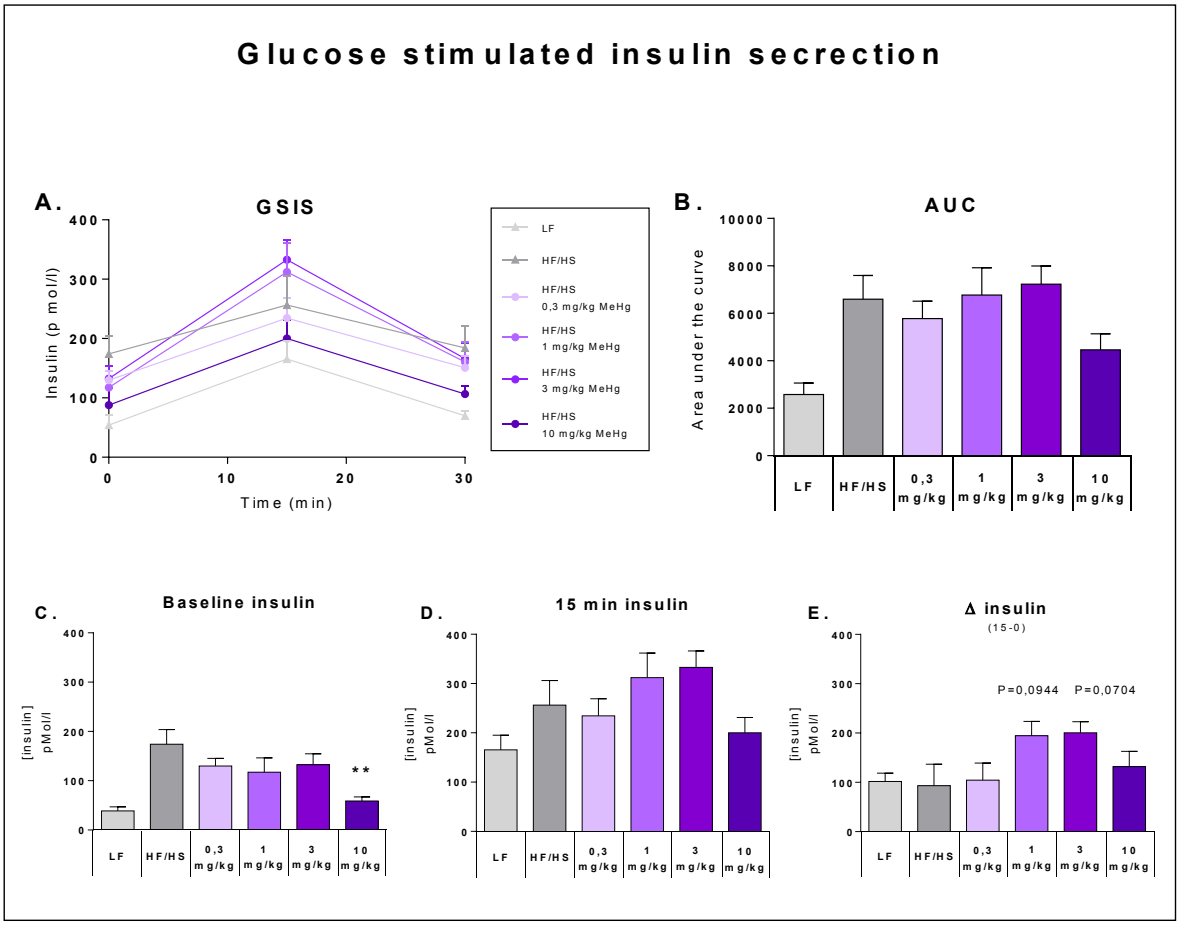

Figure 3-6. Glucose stimulated insulin secretion (GSIS). Repeated measurements ANOVA not significant A: Levels of insulin in all experimental groups at baseline, 15 and 30 minutes after glucose administration. B: Area under the curve C: Basal insulin concentrations D. Plasma insulin concentration 15 minutes after glucose administration. E: Delta insulin (15-0 minutes). All values expressed as mean ± SEM. * Refer to significant differences from non-supplemented high fat/high sucrose group according to posthoc. Dunnet's test (*P<0.05, **P<0.005). P refer to a trend (P=0.05-0.1).

Methyl mercury significantly decreased basal insulin levels of mice fed 10 mg/kg MeHg, compared to HF/HS control (Fig. 3-6 C). Although not significant, 10 mg/kg had the lowest glucose stimulated insulin secretion at all times, while 1 mg/kg MeHg and 3 mg/kg MeHg had the most elevated glucose stimulated insulin levels.

AUC of the GSIS curves tended to be higher in 1 mg/kg and 3 mg/kg, but not significantly elevated (3-6 B). 15 minutes after glucose administration, insulin levels were highest in mice exposed to 1 mg/kg and 3 mg/kg and lowest in the 10 mg/kg MeHg group, but no significant differences were observed (Fig. 3-6 D). Also when assessing delta insulin, 1 mg/kg and 3 Mg/kg MeHg mice displayed a tendency towards elevated insulin levels compared to HF/HS. When comparing all MeHg diets by repeated measurements ANOVA, we observed no significant differences on glucose stimulated isnulin secretion (3-6 A).

3.7 Effects of Methylmercury on insulin tolerance in mice

To explore the potential effect of MeHg on the development of insulin resistance, an insulin tolerance test (ITT) was performed. An intraperitonal insulin injection was given to the mice in fed state and the ability of insulin to remove glucose from the blood was measured. To assess insulin resistance, HOMA-IR was calculated. The effects of methyl mercury on insulin tolerance are shown in fig. 3-7.

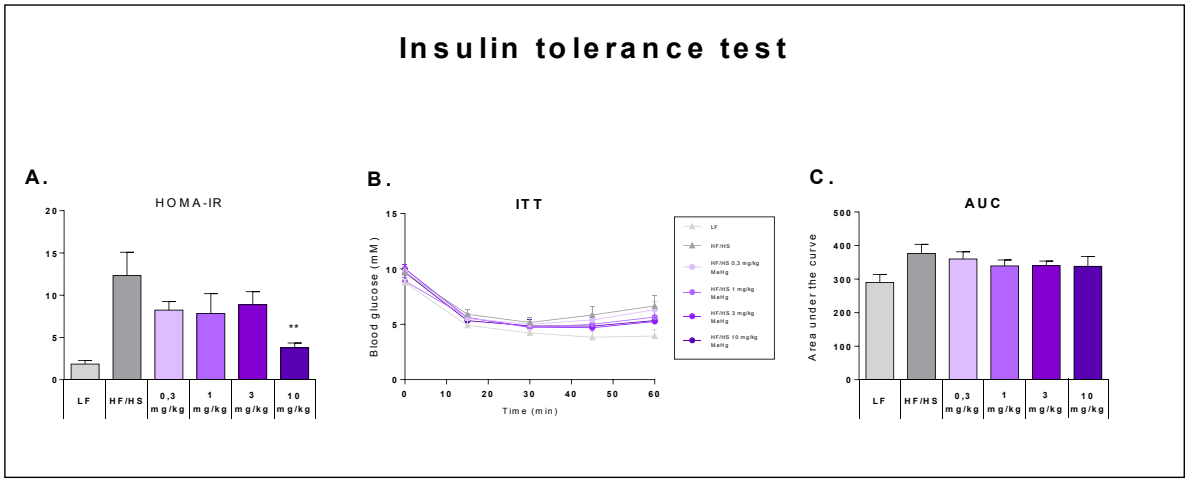

Figure 3-7. ITT performed after 10 weeks of methyl mercury exposure. A: HOMA-IR. B: The alteration of blood glucose after insulin administration. Repeated measurements ANOVA not significant. C: Area under the curve. All values expressed as mean ± SEM. * Refer to significant differences from non-supplemented high fat/high sucrose group according to posthoc. Dunnet's test (*P<0.05, **P<0.005).

MeHg did not significantly impair insulin resistance in mice at any of the exposure regimens according to repeated measurements ANOVA (Fig. 3-7 B). On that note, baseline glucose levels were approximately 8-10 mMol/L across the groups followed by a rather synchronous decline towards thirty minutes, and a slight elevation after thirty minutes. (Fig. 3-7 B). One hour after the glucose administration, HF/HS control had the highest blood glucose levels and 10 mg/kg fed mice had the lowest, although not significant. Thereby, displaying the same pattern as seen in body weight development. AUC under the ITT curves were not significantly different in the MeHg exposed groups, compared to HF/HS control (Fig 3-7 B).

When assessing HOMA-IR, mice fed the highest exposure regimen (10 mg/kg MeHg) displayed significantly higher insulin sensitivity, compared to HF/HS (Fig. 3-7 A). Again, suggesting that insulin sensitivity might be inversely associated with body weight.

3.8 Relative gene expression in mouse liver

The liver plays a major role in metabolic regulation and detoxification of pollutants, thus representing a central organ in the metabolism of nutrients like lipids and glucose in addition to degradation of toxic chemicals. HF/HS diets are known to cause obesity and metabolic disorders, such as the onset of hepatosteatosis and changes in expression of genes involved in lipid, glucose metabolism and inflammation. The livers from randomly fed mice were used to purify RNA and measure relative gene expression, to explore the impact of MeHg exposure on gene expression (Fig. 3-8).

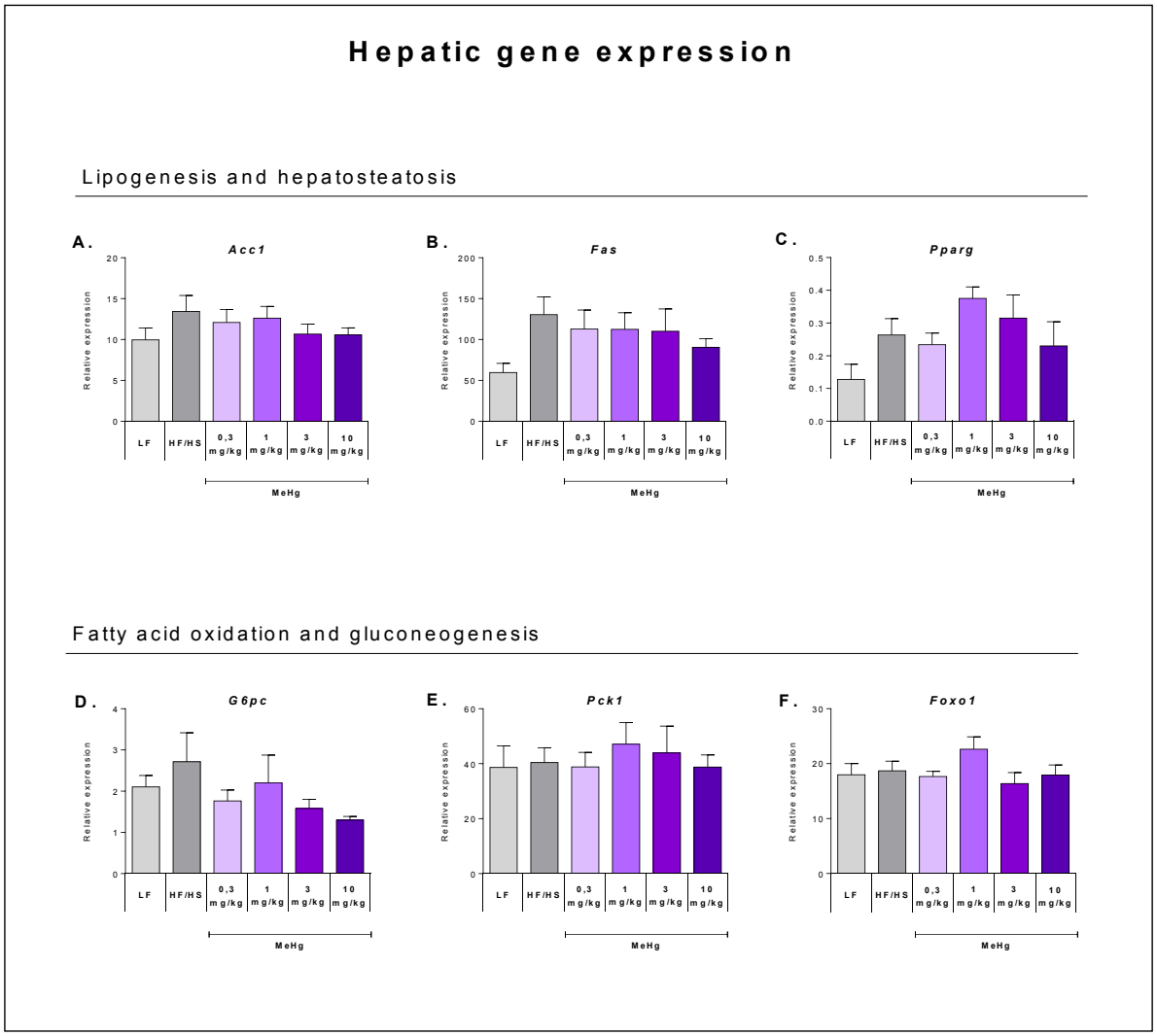

Figure 3-8. Effect of MeHg on expression of genes involved in metabolic regulation, relative to that of TATA binding protein (TBP) (housekeeping gene). A: Acc1. B: Fas. C:Ppar γ. D: G6pc. E: Pck1 F: Foxo1. All values expressed as mean ± SEM. * Refer to significant differences from non-supplemented high fat/high sucrose group according to posthoc. Dunnet's test (*P<0.05).

Unexpectedly, high fat/high sucrose feeding, did not significantly alter the gene expression of key genes involved in hepatosteatosis nor lipogenesis, regardless of contamination pressure (Fig. 3-8 A-C). Similarly, expression of genes involved in fatty acid oxidation and gluconeogenesis did not differ significantly in response to progressive MeHg exposures (Fig. 3-8 D-F). Additional genes were assessed, yet no significant differences were detected (Appendix V: Figure A2 and A3).

3.9 The fecal excretion of mercury

To explore the elimination of MeHg at different exposures, feces was collected and subsequently analyzed using direct mercury analysis (DMA80). Fecal Hg concentrations after three and nine weeks are presented in Figure 3-9.

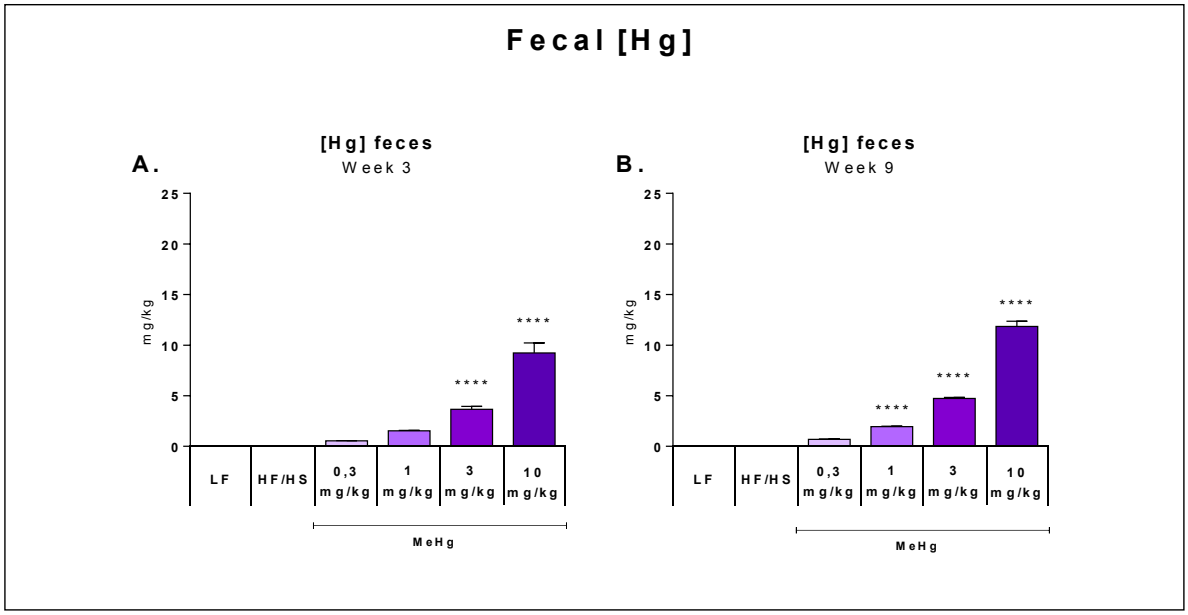

Figure 3-9. After 3 and 9 weeks of feeding on MeHg-containing diets, total mercury content was quantified in feces (mg/kg Hg). A: Fecal Hg after 3 weeks. B: Fecal Hg after 9 weeks. All values expressed as mean ± SEM. * Refer to significant differences from non-supplemented high fat/high sucrose group according to posthoc. Dunnet's test (*P<0.05, **P<0.005, ***P<0.0005, ****P<0.0005).

The fecal secretion of mercury (Hg) increased concomitantly with MeHg concentrations in the diets (Fig 3-9). After 3 weeks of exposure, the amount of MeHg in feces was significantly higher in the 3mg/kg and 10 mg/kg group compared to the non-supplemented HF/HS control (Fig. 3-9 A). 6 weeks later, MeHg secretion occurred in the same pattern, and was still significantly elevated with progressive MeHg exposures (Fig 3-9 B). Indicating that the elimination of mercury was relatively stable throughout the experiment.

3.10 Organ masses and tissue accumulation in methylmercury exposed mice

To examine if dietary exposures influenced on the organ mass of the mice, organs were dissected out and weighed. To gain further insight on the distribution of mercury in the body, the cumulative effects of MeHg were assessed in several organs. Hg accumulation was investigated by direct mercury analysis (DMA80) The mass (g) and Hg accumulation of liver, pancreas, muscle and eWAT are presented in fig. 3-10.

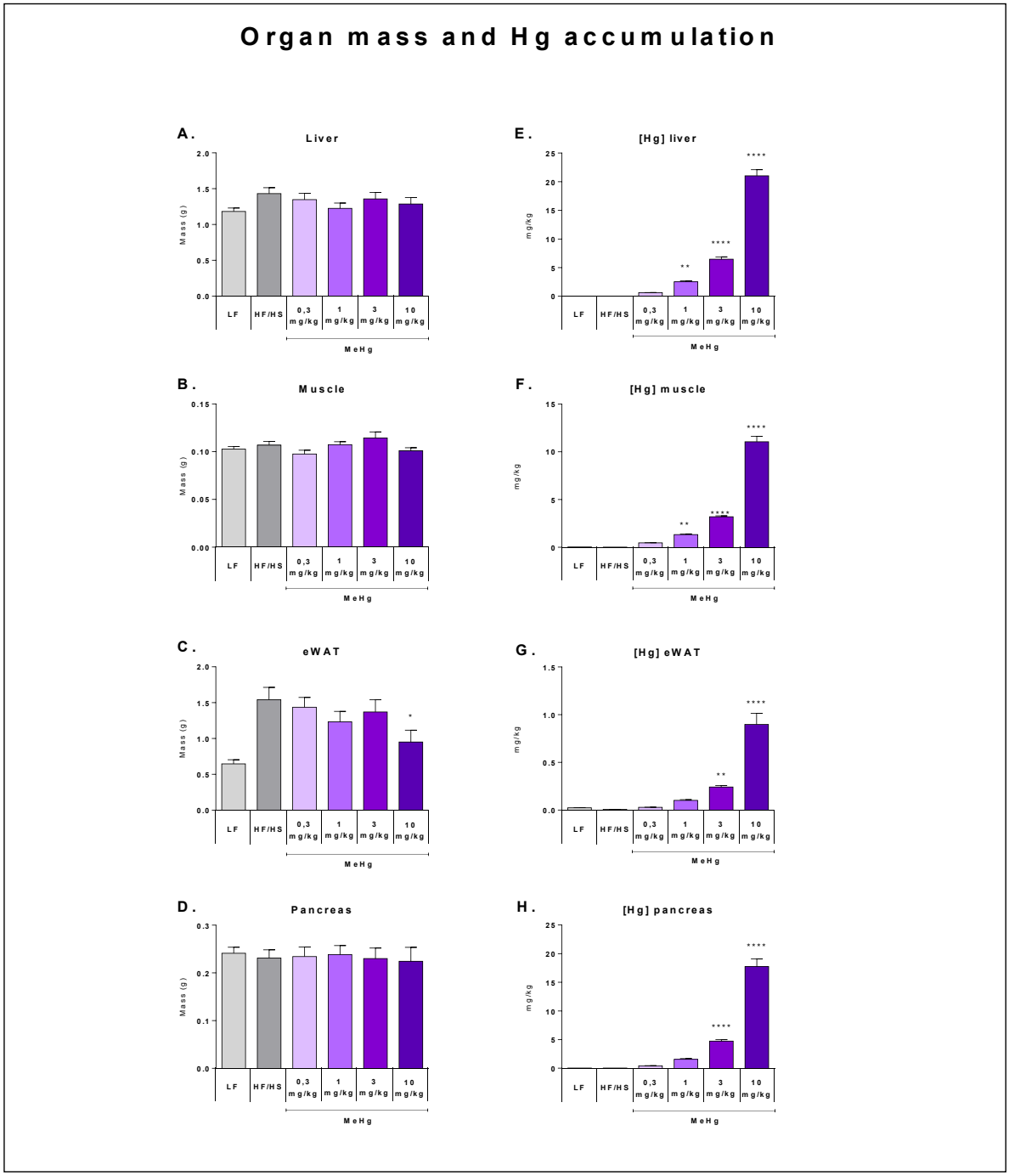

Figure 3-10. Effects of progressive MeHg exposures on organ masses and tissue accumulation. A: Liver mass (g) B: Muscle mass (g) C: eWAT mass (g). D: Pancreas mass (g) E: [Hg] Liver (mg/kg) F: [Hg] Muscle (mg/kg). G: [Hg] eWAT (mg/kg) H: [Hg] Pancreas (mg/kg). All values expressed as mean ± SEM. * Refer to significant differences from non-supplemented high fat/high sucrose group according to posthoc. Dunnet's test (*P<0.05, **P<0.005, ***P<0.0005) ****P<0.0005).

MeHg proclaimed no effects on liver-, pancreas- and muscle mass in mice, regardless of contamination pressure (Fig. 3-10 A, B and D). However, 10 mg/kg MeHg fed mice exhibited a significant decrease in eWAT (Fig. 3-10 C). Furthermore, MeHg did not alter organ masses of kidney, spleen and heart, at any exposure (Appendix V: Figure A4).

Tissue accumulation of mercury (Hg) corresponded to the dietary exposure. Direct mercury analysis revealed that the majority of MeHg fed mice had significantly increased [Hg] levels in organs, when compared with levels found in the control group. Mercury content found in liver tissue was higher than that found in other organs, and 21.03±1.068 mg/kg had accumulated in the liver of mice fed the highest dose (Fig.3-10 E) Representing a 40-fold increase compared to the lowest dose. Rather similar amounts were found in the pancreatic tissue of mice fed the highest dose, 17.74±1.320 mg/kg MeHg (Fig. 3-10 H). Furthermore, 11.06±0.5707 mg/kg and 0.89±0.1155 mg/kg MeHg was found to accumulate in muscle and eWAT, respectively (Fig 3-10 F/G).

3.11 Pancreas histology

Effects of MeHg on apoptosis in pancreatic tissue

A reduction of basal insulin levels in the 10 mg/kg MeHg group, and a substantial accumulation of Hg in pancreas led to the evaluation of the pancreatic cells. To investigate if MeHg exposure had an effect on pancreatic cells, mouse tissue from the HF/HS group and 10 mg/kg group, were stained with a fluorescent dye (Hoechst 33258) and viewed in a microscope. Images were assessed in order to detect apoptosis visualized as very bright nuclei (Condensed chromatin) or fragmented nuclei (DNA degradation), signs that the cells were preparing for programmed cell-death. Figure 3-11 show two representative pictures from the group with the highest exposure to MeHg compared to the HF/HS control group.

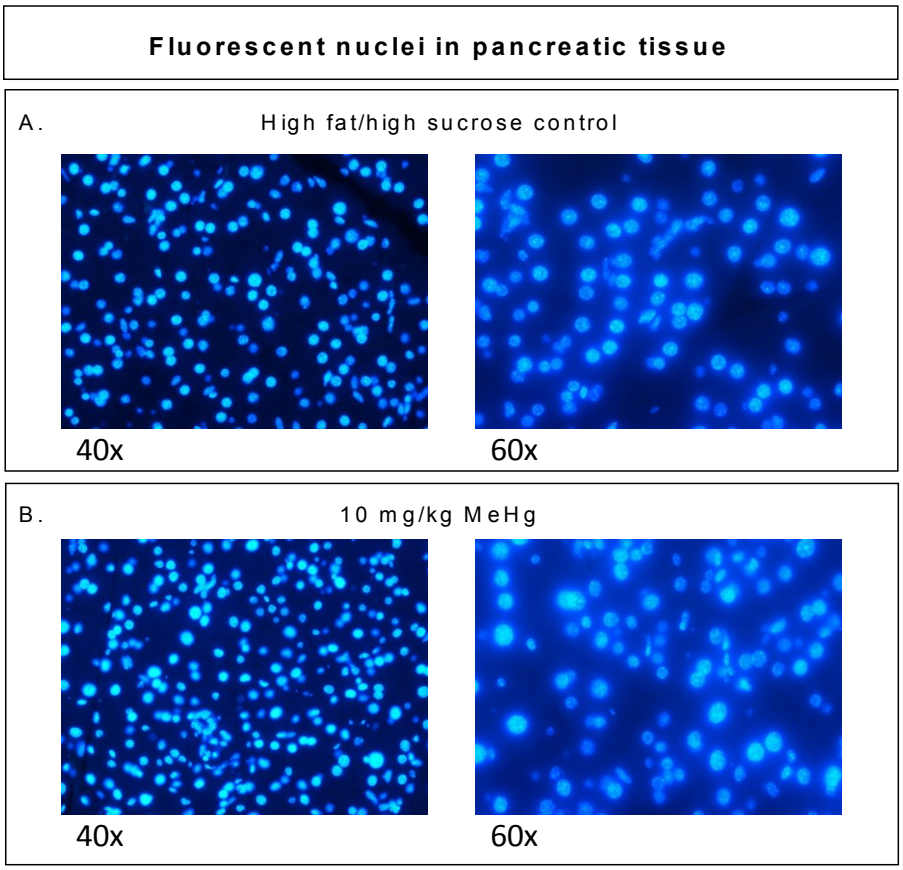

Figure 3-11. Effects of MeHg on pancreatic cell nuclear morphology, stained with Hoechst 33258 and visualized using fluorescence microscopy. A: Images from non-supplemented HF/HS control group. B: Images from 10 mg/kg MeHg group. Magnification of 40x and 60x is presented from both groups.

Initially, twenty random tissue sections from mice exposed to 10 mg/kg MeHg and HF/HS control was compared, and a selection of these are shown in Appendix VI: Figure A5. The tissue sections were thoroughly assessed and compared, but no apparent differences were observed in the nuclei of the pancreatic cells of mice exposed to 10 mg/kg versus. HF/HS control (Figure 3.11 A-B).

Effects of methylmercury on pancreatic islet masses

To evaluate the potential effects of MeHg on pancreas islet mass, pancreatic tissue was stained with eosin/hematoxilin. Islet masses were quantified in the 10 mg/kg MeHg group versus the HF/HS control, by measuring the total tissue area and the total area of the islets, using Image J. Mice from each group were randomly selected. Langerhans islets of the pancreas in two representative sections are presented in fig. 3-12.

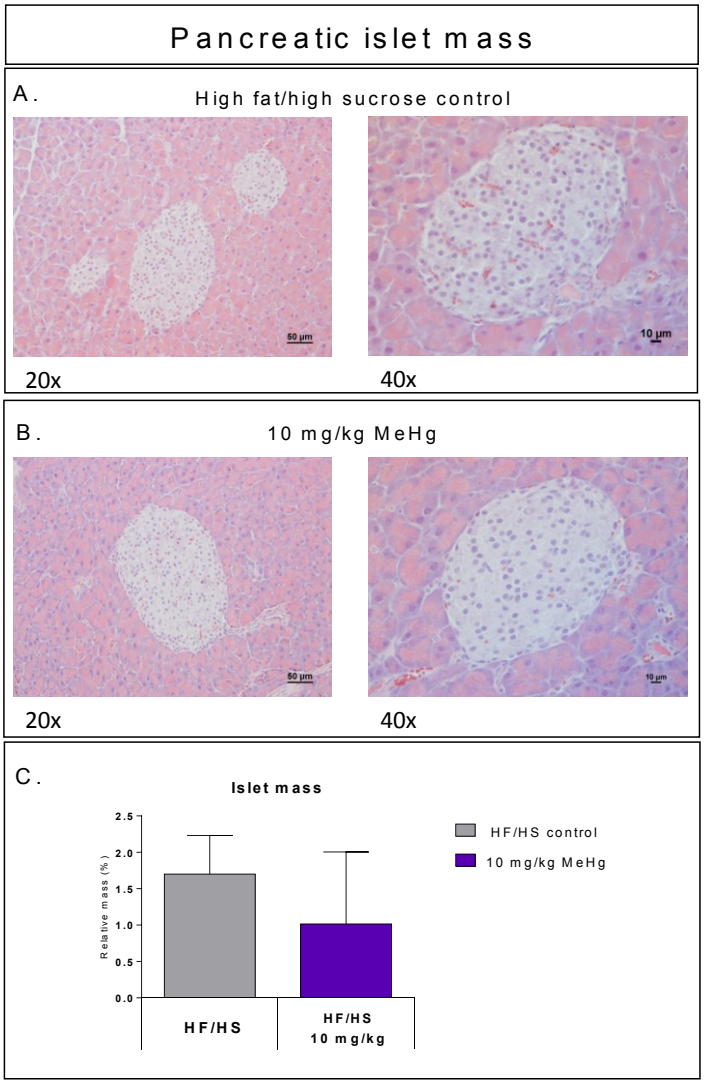

Figure 3-12. Pathological examination of Langerhans islets in the pancreas of one representative mice from the HF/HS control group and the 10 mg/kg group, visualized by staining. One 20x (scale bar = 50µm) and 40x (scale bar = 10 µm) magnification from each group. A: HF/HS group (n=4) B: 10 mg/kg (n=3). C: Islet mass quantification in the non-supplemented HF/HS versus 10 mg/kg MeHg exposure.

When assessing pancreatic tissue sections, no prominent differences were observed between the 10 mg/kg MeHg exposed group and non-supplemented HF/HS control (Fig. 3-12 A/B). Further assessment was facilitated by quantification of the islet masses of each section. No significant differences in the islet masses were observed, when comparing 10 mg/kg exposed mice, to HF/HS control (Fig. 3-12 C). Still, there was a slight decrease in islet mass in mice fed 10 mg/kg, and variation was greater in mice exposed to 10 mg/kg (non-significantly). Moreover, a visual examination of the entire sample collection might have indicated lower cells density in the pancreatic tissue of mice exposed to a contamination pressure of 10 mg/kg versus non-supplemented control. A minor selection of additional images are shown in Appendix VI: Figure A6.

4 Discussion

The purpose of this study was to investigate the potential effects of methylmercury (MeHg) on development of obesity and type 2 diabetes, as well as mercury accumulation in several tissues of the body. Obesity have reached epidemic proportions and is closely accompanied by type 2 diabetes and recent findings elucidate the role of environmental contaminants as metabolic and endocrine disruptors, potentially leading to hypoinsulinemia and type 2 diabetes (Grandjean et al., 2011; Sharp, 2012) Moreover, it has been reported that both organic mercury (Chen et al., 2006a) and inorganic mercury (Chen et al., 2006c) induce pancreatic β-cell dysfunction, through several mechanisms impinging on insulin secretion.

In fish and seafood, mercury mainly exists as MeHg; therefore, an obesogenic high fat/high sucrose (HF/HS) diet was augmented with increasing amounts of MeHg-cysteine complex. MeHg contents in the feed were ranging from 0.3 mg/kg -10 mg/kg. These high contamination pressures were used to advocate an effect in mice during a limited period. Apparent toxicity was not observed in any of the exposure regimens throughout the feeding trial.

In this study, our results showed that 10 mg/kg MeHg attenuated diet-induced obesity and reduced basal insulin levels in mice, with no concomitant reduction in glucose tolerance, insulin sensitivity or glucose stimulated insulin secretion. Furthermore, we found a dose-dependent accumulation of mercury in organs, with the highest levels found in liver and pancreas.

4.1 The influence of methylmercury on body weight development

Contradictory to our assumptions that MeHg would exaggerate obesity when added to an obesogenic HF/HS diet, the present study shows no dose-dependent increase in obesity. In fact, our results indicate that MeHg has a suppressive effect on weight gain in the intermediate (1 mg/kg) and the highest experimental dose (10mg/kg), despite being fed obesogenic HF/HS diets. The non-supplemented HF/HS control group gained the most weight, considering all groups. These differences in body weight could not be explained by alterations in total feed intake, because the feed intake was similar between the groups. It appears that the 10 mg/kg MeHg group had significantly lower feed efficiency, gaining less weight on the same amount of feed when compared to HF/HS control. Simultaneously, rejecting the suspicion that lower

weight gain was caused by depressed appetite attributable to MeHg toxicity. Reduced body masses were associated with lower adipose tissue mass. When assessing whole-body composition: the 10 mg/kg MeHg group had a significant decline in fat mass compared to HF/HS control. The lean mass of the animals did not decrease, confirming that the low weight gain was not due to food deprivation. In agreement with the modest weight gain at the highest exposure (10 mg/kg), the weight of visceral and subcutaneous fat depots were lower and the abdominal fat tended to decrease, compared to non-supplemented control. Because mice exhibited dissimilar feed efficiency at the different mercury exposures, we speculated whether this energy was eliminated through feces. The exposures that revealed a decrease in feed efficiency did not differ, when assessing fat absorption. Thus, indicating that energy was not excreted. Reduced feed efficiency in mice fed 1 mg/kg MeHg and 10 mg/kg MeHg compared to HF/HS, could possibly suggest an increase in metabolic activity due to MeHg exposure.

To gain further insight, we measured the gene expression of energy demanding processes involved in gluconeogenesis and lipolysis. Gene expression levels did not differ among the groups of MeHg exposure, therefore it is not likely that energy expenditure was increased due to theses energy consuming processes. Considering the lack of knowledge about energy expenditure in this experiment, this is simply speculative.

One can only speculate on the potential mechanisms capable of attenuating diet-induced obesity in diets spiked with MeHg. Kawakami et al. suggested that a reduction in adipocyte size due to in vivo exposures to inorganic mercury generates functional abnormalities in adipose size, proposing that the toxic effects of MeHg may contribute in the reduction of white adipose tissue depots (Kawakami et al., 2012). Other proposed mechanisms of obesity development due to MeHg exposure is based on the effects of MeHg on insulin. (Chen et al., 2006b). Insulin has three sulfur binding sites, which easily binds to mercury and might interfere in the regulation of blood glucose. In the present investigation, we found a decrease in basal insulin levels at the highest exposure, which may have prevented the obesogenic actions of the HF/HS diets. It has recently been suggested that high insulin levels are essential in HF-diet-induced obesity (Hao et al., 2012). Moreover, the fact that insulin-receptor knockout mice are protected from diet-induced obesity, indicate that insulin signaling in adipocytes is essential for obesity development (Bluher et al., 2002). MeHg potentially mediates its effects on energy metabolism by altering intracellular calcium concentrations in pancreatic β-cells (Zhou et al., 1998). Numerous mechanisms have been suggested in trying to explain the possible association

between obesity and contaminants; mainly through interruption of energy homeostasis, glucose and lipid metabolism and regulation of adipogenesis. (Kelishadi et al., 2013; Newbold, 2010). Nevertheless, exact target tissues are unknown; adipose tissues and endocrine cells communicates with endocrine signals from many organs which may involve brain, liver, gut and pancreas. Nonetheless, these reviews have not targeted MeHg in particular, but might give an indication of potential explanations for how MeHg might impinge on weight development and metabolism.

4.2 The effects of methylmercury on metabolic processes

In the present study, MeHg was not associated with obesity. I order to investigate the exerted effects on metabolic regulation, a glucose tolerance test and insulin tolerance test was performed, and some genes affecting these processes were explored.

Our results displayed a decrease in glucose tolerance among mice fed the lowest exposure dose (0.3 mg/kg MeHg). Fasted glucose levels were rather similar across groups, indicating no state of hyperglycemia, found in type 2 diabetes. In addition, 0.3 mg/kg MeHg fed mice remained insulin sensitive, probably coincident with the moderate weight gain. In fact, all groups remained insulin sensitive, regardless of contamination pressures, suggesting no negative association between MeHg and insulin secretion.

MeHg significantly reduced basal insulin levels in mice fed 10 mg/kg, compared to non-supplemented HF/HS. However, no significant alterations were detected in glucose stimulated insulin secretion among the groups. Unexpectedly, basal blood glucose was not elevated due to reduced basal insulin levels in the 10 mg/kg MeHg group. The latter did not develop insulin resistance and according to HOMA-IR calculations, 10 mg/kg methyl mercury fed mice were highly insulin sensitive. This is in line with the fact that 10 mg/kg exposed mice remained lean. Regardless of the complexity of these interactions, it is not to be dismissed that a decline in basal glucose levels, might indicate a reduced ability of the β-cells to produce insulin. Pathological alterations in pancreas capable of inducing endocrine disturbances was already described in 1977, when Takeuchi et al. found perturbations in the epithelium of pancreatic islet cells in autopsy cases of Minamata disease (Takeuchi T and Eto K, 1977). Although not significant, our results displayed a rather consistent pattern in glucose stimulated insulin secretion across the groups, in which insulin levels increased from 0.3 mg/kg to 3 mg/kg

followed by a decline at the highest exposure regimens. The intermediate-exposures (1 mg/kg and 3 mg/kg) tended to increase glucose stimulated insulin secretion. It has been suggested that some contaminants exert a low dose stimulation, high dose inhibition displaying an inverted u-shaped dose response. (Calabrese and Baldwin, 2003). Thus, acting to improve physiological parameters at low doses, followed by an deterioration at higher exposures. In addition to the possibility that MeHg could act stimulatory at low doses, and inhibitory at high doses, some toxicological studies have demonstrated non-monotonic dose responses (Welshons et al., 2003). Recently, Chang et al. found that dioxin exposure was associated with a slight monotonic increase in insulin resistance in Taiwanese living in a highly polluted area (Chang et al., 2011). It might not be possible to predict responses in low dose exposures, based on exposures in a high range, underlining the fact that dose responses are ambiguous (Newbold, 2010). Further, our finding that mice receiving the lowest dose (0.3 mg/kg) exhibited glucose intolerance might indicate that the effects of MeHg differ in the low region exposures, compared to higher. Subsequently raising the question whether even lower doses could trigger more adverse effects on different metabolic markers. For instance, Chen et al. found that low doses of MeHg was capable of modifying glucose tolerance and insulin secretion after 4 weeks in vitro. (Chen et al., 2006c).

In the current experiment, MeHg was not associated with insulin resistance. Insulin resistance is closely related to obesity, therefore the modest weight gain in all groups might partly explain why the mice remained insulin sensitive (Xu et al., 2003). However, we measured whole body non-specific insulin sensitivity, and thus, indications about the insulin sensitivity of individual organs are restricted. Further, we do not know if a pro-longed exposure, at the same or other doses, would have triggered insulin resistance, and glucose intolerance. An increase in adipose tissue, would possibly have lead to increased levels of free fatty acids which in turn might lead to resistance to insulin signaling in liver and muscle (Yu et al., 2002). Recently, Yamamoto et al. found that body fat gain in mice with type 2 diabetes mellitus increased the toxicity of MeHg compared to lean non-diabetic C57BL/6 mice (Yamamoto et al., 2013). We can only speculate if we had seen more adverse effects of MeHg if the mice were fat before the implementation of MeHg.

Liver is one of the target organs of MeHg and at the same time has major impact on metabolic processes, therefore very relevant when assessing obesity and diabetes. The liver masses did not differ between the treatment groups, displaying no immediate pathological alterations in

response to MeHg supplemented HF/HS diets. Further, it was evident that liver had accumulated the highest amounts of MeHg, among the organs that were analysed. MeHg is known to accumulate extensively in the liver, and among other organs like the brain and kidneys (Bridges and Zalups, 2010; Rodrigues et al., 2010). Interestingly, Roos et al. found that exposures to MeHg-cys complex substantially increased accumulation in liver, when compared to MeHg alone (Roos et al., 2010). Due to the high accumulation in liver, hepatic gene expression was explored. Assessments of a selection of genes, did not display a transparent relationship between contamination pressure and gene expression in liver. There were no differences in genes involved in anabolic processes nor energy expending processes in the liver. This might be an indication that accumulation is not predicative of the metabolic functions of the liver. Based on these results, it is not likely that the reduction in basal insulin levels was due to alterations of gene expression in liver.

4.3 Methylmercury accumulation and pancreatic function

In the current investigation, MeHg was associated with a reduction in basal insulin secretion in response to a contamination pressure of 10 mg/kg. Based on this finding we speculate if MeHg could have negative effects on the ability of pancreas to secrete insulin.

Pancreas masses did not differ among the treatment groups, displaying no obvious pathological change in the organ mass due to MeHg exposure. In line with others that have investigated accumulation in liver, our results show that the hepatic burdens are highest when exposed to MeHg-cysteine complex, as opposed to MeHg alone (Roos et al., 2010). It has been suggested that the high accumulation might be related to the protein metabolic properties of the liver, receiving amino acids from the gastrointestinal tract and other organs (Adachi, 2006). When comparing the accumulation of MeHg in the different organs, it was evident that pancreas accumulated nearly as much as liver, whereas muscle displayed only half of the burden found in liver and pancreas. Only small amounts accumulated in eWAT, similar to what has been found in other studies (Nielsen, 1992; Yamamoto et al., 2013). Overall, the investigated organs displayed an increase in MeHg in which the highest exposure yielded the highest burden.

Surprisingly, we found that pancreas accumulated high concentrations of MeHg. To our knowledge, investigations on the cumulative properties of MeHg in mice pancreas is restricted. However, Yamamoto et al. recently explored the total mercury concentrations in pancreas of C57BL/6 mice and diabetic KK-AY mice after MeHg administration through oral gavage

(Yamamoto et al., 2013). In their study, kidneys accumulate the most MeHg, followed by pancreas and liver. Additionally, the obese diabetic KK-AY mice had much greater accumulation in pancreas and liver than the lean non-diabetic C57BL/6 control mice, suggesting that body weight gain might be a predictor for MeHg susceptibility and individual differences in response to contamination. Whereas the current experiment added MeHg-cys to feed, Yamamoto et al. administered MeHg without a food matrix. Given that the route of exposure differs from the present investigation, we speculate if uptake and distribution may differ. There are many factors conflicting the basis for comparison between studies; emphasizing the importance of mimicking the normal human exposure route and relevant mercury species, to obtain a more realistic view on accumulation in target organs.

The accumulation of MeHg in target organs could possibly reflect the burdens observed, but is not predicative of a pathological outcome. Considering that pancreas is the organ responsible for insulin secretion, it is also a representative target organ for diabetes. Therefore, we explored the pancreatic tissue of mice at the highest exposure level (10 mg/kg), through histological methods. We found no signs of apoptosis when comparing the non-supplemented HF/HS control group and 10 mg/kg MeHg exposed mice. We cannot exclude the possibility that apoptosis occurred in the pancreatic tissues based on these observations alone. Although we made no observations on condensed nuclei, apoptosis may have occurred in the cells of pancreas. If we had used early apoptotic markers to detect apoptosis, this could have provided knowledge in regards of the regulation of apoptotic proteins. Thus highlighting that the current observations are by no means conclusive in regards of MeHg effect on cells of the pancreas. Previous studies have demonstrated the ability of MeHg to induce β-cell dysfunction and cell apoptosis through an oxidative stress pathway in mice. The same group of scientists reported that activation of the PI3K- pathway caused β-cell dysfunction through an AKT signaling pathway and thereby decreasing insulin secretion, suggesting that exposure to mercury may be a risk factor for diabetes (Chen et al., 2006b; Chen et al., 2006c; Chen et al., 2010). An experiment in rats have reported that a single injection of MeHg was capable of damaging pancreatic islets, and that repeated injections triggered high glucose levels (Shigenaga, 1976).

To gain further insight on the potential interferences of MeHg in pancreatic tissues, we investigated the islets of pancreas. We observed no apparent morphological alterations in the islets, and the different sections displayed no obvious difference in islet mass, comparing 1 mg/kg, 10 mg/kg and the HF/HS control group. Further we quantified the islet mass in randomly

selected tissues within the HF/HS control group and 10 mg/kg. Although non-significant, islet mass was slightly lower in the 10 mg/kg group and the variation within the this group was slightly higher, compared to HF/HS control. This might be an indication that some mice responded to the exposures, whereas others did not. Further examinations of all sections indicated that there might be a slight decrease in cell density in islets of the pancreas at the highest exposure regimen, compared to non-supplemented HF/HS control.

In human studies, the potential role of MeHg in development of diabetes have been elucidated and findings are contradictory. A cross sectional study from the Faroese population reported that exposures to contaminants, impaired insulin secretion in 70 year olds, which is an important part of type 2 diabetes pathogenesis (a population with high consumption of pilot whale) (Grandjean et al., 2011). Findings from the Coronary Artery Risk Development in Young Adults (CARDIA) study, recently reported an association between high methylmercury exposures in young adulthood and higher risk of diabetes later in life (He et al., 2013). In 1995 a retrospective study suggested that an increase in incidence diabetes seen in Minamata disease might be explained by high methylmercury exposures (Uchino et al., 1995). However, conflicting evidence was recently reported from two separate large prospective cohorts, reporting no adverse effects of MeHg on development of diabetes. (Mozaffarian et al., 2013) Equally, an epidemiological study in a population living in a MeHg polluted area showed no increase in diabetes mellitus (Futatsuka et al., 1996). Regardless, more research is required to elucidate the role of MeHg on type 2 diabetes.

4.4 Human relevance

Fish and seafood is an important part of a healthy diet because it contains many beneficial nutrients (Strain et al., 2008; VKM, 2006). Some nutrients in seafood may have ameliorating effects on MeHg toxicity, among them selenium and Omega 3 (Folven et al., 2009; Nostbakken et al., 2012). In the present investigation the beneficial nutrients in fish and seafood was not accounted for, and a holistic risk-benefit evaluation is required to assess the effects of MeHg through seafood consumption. The exposures in the present experiment is not comparable to human consumption because the mice were chronically exposed to MeHg through every meal, whereas humans eat a variety of foods. Although, the lowest dose (0.3 mg/kg) is similar to that found in some freshwater fish (pike, trout, perch) and 1-3 mg/kg might be found in some predatory fish (Greenland halibut, tuna) and deep water fish species (tusk) in particular areas.

However, the consumption of these species are considered low, although not excluding the fact that some groups in the population might consume these species at a regular basis.

4.5 The animal model

The mice model is frequently used in scientific research because of their similarity to humans in terms of genetics, anatomy and physiology. Moreover, the given opportunity to control an experiment is of great value in achieving scientifically valid research. However, caution must be taken in translating the outcome to humans. Whereas features of the inbred strain is desirable when controlling the experiment, inbreeding gives less genetic variation somewhat compromising human resemblance. Thus, underlining the importance of restriction when generalizing findings.

The mouse model is valuable in providing insights into aspects of toxicity otherwise impossible to investigate. C57BL/6 is an appropriate model when assessing obesity and diabetes, however, there are several mouse models that might be more appropriate when assessing contaminants like MeHg. In the current investigation, C57BL/6 mice demonstrated profound endurance against the high dose exposures. Other mice-strains might be more susceptible to MeHg and might exhibit toxic responses much earlier. BALBc is commonly used in toxicology studies, and a recent study using KK-AY mice demonstrated high susceptibility to MeHg exposure(Yamamoto et al., 2013).

4.6 Methodology

Feed production

Obesity development was evaluated on the basis of a 13 week feeding trial. Production of feed was part of the laboratory training. Due to the fact that the feed production consisted into the feeding trial and consisted of several batches, the consistency of the feed was varying in the first weeks of feeding. This might have resulted in a weight gain advantage for the mice receiving a consistent diet, and a stressor for the counterpart. Diets were analyzed for MeHg, fat, protein, displaying similar contents. For future experiments, it would be beneficial to prepare and analyze the diets prior to the feeding trial, to ensure a homogenous feed accessibility for the animals at all times. Since feed intake was comparable among the groups, it is not likely that this had an impact on the outcome of our experiment. Based on experience from parallel experiments, the ability to induce obesity might also be dependent on the physical

form of the diet; Pellet vs. powdered feed. Findings from a recent study in C57BL/6 mice showed a greater increase in body weight when fed a powdered diet, than mice fed the pelleted diets (Yan et al., 2011).

5 Conclusions

In vivo, chronic exposures to progressive (0.3 mg/kg, 1 mg/kg, 3 mg/kg and 10 mg/kg) methylmercury-cysteine concentrations, supplemented to an obesogenic high fat/high sucrose diet, did not induce obesity development in C57BL/6 mice, however:

- The highest MeHg exposure (10 mg/kg) attenuated diet-induced obesity and reduced basal insulin secretion.
- Mercury accumulated dose-dependently in several organs, with the highest levels accumulated in liver and pancreas.
- MeHg induced a modest decline in glucose tolerance at the lowest exposure regimen (0.3 MeHg) but was not associated with reduced insulin sensitivity or reduced glucose stimulated insulin secretion.

5.1 Future perspectives

Due to the accumulation of mercury in pancreas and reduced basal insulin secretion at the highest exposure, it would be interesting to:

- Locate the sites for accumulation, through mercury specific staining in pancreatic tissue and investigate if there is a selective accumulation in pancreatic β-cells.
- Isolate primary islets and expose to methylmercury to investigate the effect on glucose stimulated insulin secretion
- Investigate the effects of methylmercury in other background diets, with pro-longed exposure, and explore the effects of lower methylmercury doses.
- Further, investigate if methylmercury induces apoptosis in pancreatic cells. For instance by investigating early apoptotic markers.

6 References

Adachi, T. (2006). Characteristic effects of L-methionine on tissue distribution of methylmercury in mice. Journal of Health Science, 174-172.

Allen, J.W., Shanker, G., and Aschner, M. (2001). Methylmercury inhibits the in vitro uptake of the glutathione precursor, cystine, in astrocytes, but not in neurons. Brain Research *894*, 131-140.

Andrikopoulos, S., Blair, A.R., Deluca, N., Fam, B.C., and Proietto, J. (2008). Evaluating the glucose tolerance test in mice. Am J Physiol Endocrinol Metab *295*, E1323-1332.

Atchison, W.D., and Hare, M.F. (1994). Mechanisms of methylmercury-induced neurotoxicity. FASEB J *8*, 622-629.

ATSDR (1999). ToxFAQsTM for Mercury (Atlanta).

Bakir, F., Damluji, S.F., Amin-Zaki, L., Murtadha, M., Khalidi, A., al-Rawi, N.Y., Tikriti, S., Dahahir, H.I., Clarkson, T.W., Smith, J.C*., et al.* (1973). Methylmercury poisoning in Iraq. Science *181*, 230-241.

Betty L. Black, J.C., E.J. Eisen, Ann E. Petro, Christopher L. Edwards, Richard S. Surwit, (1998). Differential effects of fat and sucrose on body composition in AJ and C57BL/6 mice. Metabolism *Volume 47*, 1354-1359

Bluher, M., Michael, M.D., Peroni, O.D., Ueki, K., Carter, N., Kahn, B.B., and Kahn, C.R. (2002). Adipose tissue selective insulin receptor knockout protects against obesity and obesity-related glucose intolerance. Dev Cell *3*, 25-38.

Bray, G.A. (2004). Medical Consequences of Obesity. The Journal of Clinical Endocrinology & Metabolism *89*, 2583-2589.

Bridges, C.C., and Zalups, R.K. (2010). Transport of inorganic mercury and methylmercury in target tissues and organs. J Toxicol Environ Health B Crit Rev *13*, 385-410.

Calabrese, E.J., and Baldwin, L.A. (2003). Hormesis: the dose-response revolution. Annu Rev Pharmacol Toxicol *43*, 175-197.

Ceccatelli, S., Dare, E., and Moors, M. (2010). Methylmercury-induced neurotoxicity and apoptosis. Chem Biol Interact *188*, 301-308.

Chang, J.W., Chen, H.L., Su, H.J., Liao, P.C., Guo, H.R., and Lee, C.C. (2011). Simultaneous exposure of non-diabetics to high levels of dioxins and mercury increases their risk of insulin resistance. J Hazard Mater *185*, 749-755.

Chen, Y.W., Huang, C.F., Tsai, K.S., Yang, R.S., Yen, C.C., Yang, C.Y., Lin-Shiau, S.Y., and Liu, S.H. (2006a). Methylmercury induces pancreatic beta-cell apoptosis and dysfunction. Chem Res Toxicol *19*, 1080-1085.

Chen, Y.W., Huang, C.F., Tsai, K.S., Yang, R.S., Yen, C.C., Yang, C.Y., Lin-Shiau, S.Y., and Liu, S.H. (2006b). Methylmercury Induces Pancreatic β-Cell Apoptosis and Dysfunction. Chemical Research in Toxicology *19*, 1080-1085.

Chen, Y.W., Huang, C.F., Tsai, K.S., Yang, R.S., Yen, C.C., Yang, C.Y., Lin-Shiau, S.Y., and Liu, S.H. (2006c). The role of phosphoinositide 3-kinase/Akt signaling in low-dose mercury-induced mouse pancreatic beta-cell dysfunction in vitro and in vivo. Diabetes *55*, 1614-1624.

Chen, Y.W., Huang, C.F., Yang, C.Y., Yen, C.C., Tsai, K.S., and Liu, S.H. (2010). Inorganic mercury causes pancreatic beta-cell death via the oxidative stress-induced apoptotic and necrotic pathways. Toxicol Appl Pharmacol *243*, 323-331.

Chen, Y.W., Yang, C.Y., Huang, C.F., Hung, D.Z., Leung, Y.M., and Liu, S.H. (2009). Heavy metals, islet function and diabetes development. Islets *1*, 169-176.

Clarkson, T.W. (1972). The pharmacology of mercury compounds. Annu Rev Pharmacol *12*, 375-406.

Clarkson, T.W., L. Friberg, G. Nordberg, and P.R. Sager (1988). Biological Monitoring of Toxic Metals. .

Clarkson, T.W., and Magos, L. (2006). The toxicology of mercury and its chemical compounds. Crit Rev Toxicol *36*, 609-662.

EFSA (2012). Panel on Contaminants in the Food Chain (CONTAM). Scientific Opinion on the risk for public health related to the presence of mercury and methylmercury in food. (EFSA Journal 2012).

Eto, K. (1997). Pathology of Minamata disease. Toxicol Pathol *25*, 614-623.

Federico, A., D'Aiuto, E., Borriello, F., Barra, G., Gravina, A.G., Romano, M., and De Palma, R. (2010). Fat: a matter of disturbance for the immune system. World J Gastroenterol *16*, 4762-4772.

Ferrannini, E., Gastaldelli, A., Miyazaki, Y., Matsuda, M., Mari, A., and DeFronzo, R.A. (2005). β-Cell Function in Subjects Spanning the Range from Normal Glucose Tolerance to Overt Diabetes: A New Analysis. The Journal of Clinical Endocrinology & Metabolism *90*, 493-500.

Folven, K.I., Glover, C.N., Malde, M.K., and Lundebye, A.K. (2009). Does selenium modify neurobehavioural impacts of developmental methylmercury exposure in mice? Environ Toxicol Pharmacol *28*, 111-119.

Futatsuka, M., Kitano, T., and Wakamiya, J. (1996). An epidemiological study on diabetes mellitus in the population living in a methyl mercury polluted area. J Epidemiol *6*, 204-208.

Graff, R.D., Falconer, M.M., Brown, D.L., and Reuhl, K.R. (1997). Altered sensitivity of posttranslationally modified microtubules to methylmercury in differentiating embryonal carcinoma-derived neurons. Toxicol Appl Pharmacol *144*, 215-224.

Grandjean, P., Henriksen, J.E., Choi, A.L., Petersen, M.S., Dalgard, C., Nielsen, F., and Weihe, P. (2011). Marine food pollutants as a risk factor for hypoinsulinemia and type 2 diabetes. Epidemiology *22*, 410-417.

Hao, Q., Lillefosse, H.H., Fjaere, E., Myrmel, L.S., Midtbo, L.K., Jarlsby, R.H., Ma, T., Jia, B., Petersen, R.K., Sonne, S.B.*, et al.* (2012). High-glycemic index carbohydrates abrogate the antiobesity effect of fish oil in mice. Am J Physiol Endocrinol Metab *302*, E1097-1112.

He, K., Xun, P., Liu, K., Morris, S., Reis, J., and Guallar, E. (2013). Mercury exposure in young adulthood and incidence of diabetes later in life: the CARDIA Trace Element Study. Diabetes Care *36*, 1584-1589.

Hirayama, K. (1985). Effects of combined administration of thiol compounds and methylmercury chloride on mercury distribution in rats. Biochem Pharmacol *34*, 2030-2032.

Hirayama, K., Yasutake, A., and Adachi, T. (1991). Mechanism for Renal Handling of Methylmercury. In Advances in Mercury Toxicology, T. Suzuki, N. Imura, and T. Clarkson, eds. (Springer US), pp. 121-134.

Jurgens, C.A., Toukatly, M.N., Fligner, C.L., Udayasankar, J., Subramanian, S.L., Zraika, S., Aston-Mourney, K., Carr, D.B., Westermark, P., Westermark, G.T.*, et al.* (2011). beta-cell loss and beta-cell apoptosis in human type 2 diabetes are related to islet amyloid deposition. Am J Pathol *178*, 2632-2640.

Kahn, S.E., Cooper, M.E., and Del Prato, S. (2014). Pathophysiology and treatment of type 2 diabetes: perspectives on the past, present, and future. Lancet *383*, 1068-1083.

Kawakami, T., Hanao, N., Nishiyama, K., Kadota, Y., Inoue, M., Sato, M., and Suzuki, S. (2012). Differential effects of cobalt and mercury on lipid metabolism in the white adipose tissue of high-fat diet-induced obesity mice. Toxicol Appl Pharmacol *258*, 32-42.

Kelishadi, R., Poursafa, P., and Jamshidi, F. (2013). Role of environmental chemicals in obesity: a systematic review on the current evidence. J Environ Public Health *2013*, 896789.

Kershaw, T.G., Clarkson, T.W., and Dhahir, P.H. (1980). The relationship between blood levels and dose of methylmercury in man. Arch Environ Health *35*, 28-36.

Lancet (2011). The global obesity pandemic: shaped by global drivers and local environments. wwwthelancetcom *Vol 378*.

Layden, T.B., Durai, V., and William., L.L. (2010). G-Protein-Coupled Receptors, Pancreatic Islets and Diabetes. Nature education.

Leto, D., and Saltiel, A.R. (2012). Regulation of glucose transport by insulin: traffic control of GLUT4. Nat Rev Mol Cell Biol *13*, 383-396.

Lowell, B.B., and Shulman, G.I. (2005). Mitochondrial dysfunction and type 2 diabetes. . Science, 384-387.

MacDonald, M.J., and Fahien, L.A. (1990). Insulin release in pancreatic islets by a glycolytic and a Krebs cycle intermediate: contrasting patterns of glyceraldehyde phosphate and succinate. Arch Biochem Biophys *279*, 104-108.

Mason, R.P., Rolfhus, K.R., and Fitzgerald, W.F. (1995). Methylated and elemental mercury cycling in surface and deep ocean waters of the North Atlantic. Water Air Soil Pollut *80*, 665-677.

McCarthy, M.I. (2010). Genomics, Type 2 Diabetes, and Obesity. New England Journal of Medicine *363*, 2339-2350.

Morel, F., Kraepiel, A., and Amyot, M. (1998). The chemical cycle and bioaccumulation of mercury. Annual Review of Ecology and Systematics *29*, 543-566.

Mozaffarian, D., Shi, P., Morris, J.S., Grandjean, P., Siscovick, D.S., Spiegelman, D., and Hu, F.B. (2013). Methylmercury exposure and incident diabetes in U.S. men and women in two prospective cohorts. Diabetes Care *36*, 3578-3584.

Måge, A., Bjelland, O., Olsvik, P., Nilsen, B., and Julshamn, K. (2011). Miljøgifter i fisk og fiskevarer 2011: Kvikksølv i djupvassfisk og skaldyr frå Hardangerfjorden samt miljøgifter i marine oljer

2012 (Bergen, Nasjonalt institutt for ernærings- og sjømatforskning (NIFES)).

National Research Counsil (2011). Guide for the Care and Use of Laboratory Animals: Eighth Edition (The National Academies Press).

Newbold, R.R. (2010). Impact of environmental endocrine disrupting chemicals on the development of obesity. Hormones (Athens) *9*, 206-217.

Nielsen, J.B. (1992). Toxicokinetics of mercuric chloride and methylmercuric chloride in mice. J Toxicol Environ Health *37*, 85-122.

Nostbakken, O.J., Bredal, I.L., Olsvik, P.A., Huang, T.S., and Torstensen, B.E. (2012). Effect of marine omega 3 fatty acids on methylmercury-induced toxicity in fish and mammalian cells in vitro. J Biomed Biotechnol *2012*, 417652.

Petro, A.E., Cotter, J., Cooper, D.A., Peters, J.C., Surwit, S.J., and Surwit, R.S. (2004). Fat, carbohydrate, and calories in the development of diabetes and obesity in the C57BL/6J mouse. Metabolism *53*, 454-457.

Poitout, V., Amyot, J., Semache, M., Zarrouki, B., Hagman, D., and Fontes, G. (2010). Glucolipotoxicity of the pancreatic beta cell. Biochim Biophys Acta *1801*, 289-298.

Quinn, P.G., and Yeagley, D. (2005). Insulin regulation of PEPCK gene expression: a model for rapid and reversible modulation. Curr Drug Targets Immune Endocr Metabol Disord *5*, 423-437.

Rahier, J., Guiot, Y., Goebbels, R.M., Sempoux, C., and Henquin, J.C. (2008). Pancreatic beta-cell mass in European subjects with type 2 diabetes. Diabetes Obes Metab *10 Suppl 4*, 32-42.

Rodrigues, J.L., Serpeloni, J.M., Batista, B.L., Souza, S.S., and Barbosa, F., Jr. (2010). Identification and distribution of mercury species in rat tissues following administration of thimerosal or methylmercury. Arch Toxicol *84*, 891-896.

Rolo, A.P., and Palmeira, C.M. (2006). Diabetes and mitochondrial function: role of hyperglycemia and oxidative stress. Toxicol Appl Pharmacol *212*, 167-178.

Rooney, J.P.K. (2007). The role of thiols, dithiols, nutritional factors and interacting ligands in the toxicology of mercury. Toxicology *234*, 145-156.

Roos, D.H., Puntel, R.L., Lugokenski, T.H., Ineu, R.P., Bohrer, D., Burger, M.E., Franco, J.L., Farina, M., Aschner, M., Rocha, J.B.*, et al.* (2010). Complex methylmercury-cysteine alters mercury accumulation in different tissues of mice. Basic Clin Pharmacol Toxicol *107*, 789-792.

Saltiel, A.R., and Kahn, C.R. (2001). Insulin signalling and the regulation of glucose and lipid metabolism. Nature *414*, 799-806.

Sarafian, T., and Verity, M.A. (1991). Oxidative mechanisms underlying methyl mercury neurotoxicity. Int J Dev Neurosci *9*, 147-153.

Schaefer, J.K., Rocks, S.S., Zheng, W., Liang, L., Gu, B., and Morel, F.M. (2011). Active transport, substrate specificity, and methylation of Hg(II) in anaerobic bacteria. Proc Natl Acad Sci U S A *108*, 8714-8719.

Sharp, D. (2012). Environmental toxins, a potential risk factor for diabetes among canadian aborginals. International Journal of Circumpolar Health *68*.

Shigenaga, K. (1976). Pancreatic islet injury induced by methyl mercuric chloride light and electron microscopic studies. Kumamoto Med J *29*, 67-81.

Strain, J.J., Davidson, P.W., Bonham, M.P., Duffy, E.M., Stokes-Riner, A., Thurston, S.W., Wallace, J.M., Robson, P.J., Shamlaye, C.F., Georger, L.A.*, et al.* (2008). Associations of maternal long-chain polyunsaturated fatty acids, methyl mercury, and infant development in the Seychelles Child Development Nutrition Study. Neurotoxicology *29*, 776-782.

Surwit, R.S., Feinglos, M.N., Rodin, J., Sutherland, A., Petro, A.E., Opara, E.C., Kuhn, C.M., and Rebuffe-Scrive, M. (1995). Differential effects of fat and sucrose on the development of obesity and diabetes in C57BL/6J and AJ mice. Metabolism *44*, 645-651.

Takeuchi T, and Eto K (1977). Patology and pathogenesis of Minamata disease. Kodansha LTD, 103-141.

Tsubaki, T. (1967). Outbreak of intoxication by organic compounds in Niigata Prefecture Jpn J Med Sci Biol.

Uchino, M., Tanaka, Y., Ando, Y., Yonehara, T., Hara, A., Mishima, I., Okajima, T., and Ando, M. (1995). Neurologic features of chronic minamata disease (organic mercury poisoning) and incidence of complications with aging. J Environ Sci Health B *30*, 699-715.

VKM (2006). Norwegian Scientific Commitee for Food Safety. A comprehensive assessment of fish and other seafood in the Norwegian diet.

Welshons, W.V., Thayer, K.A., Judy, B.M., Taylor, J.A., Curran, E.M., and vom Saal, F.S. (2003). Large effects from small exposures. I. Mechanisms for endocrine-disrupting chemicals with estrogenic activity. Environ Health Perspect *111*, 994-1006.

WHO (2000). Obesity: preventing and managing the global epidemic. (Geneva).

WHO (2008). Guidance for Identifying Populations at Risk from Mercury Exposure (Geneva).

WHO (2011). Global status report on noncommunicable diseases 2010, W.h. oranization, ed., pp. 176.

Xu, H., Barnes, G.T., Yang, Q., Tan, G., Yang, D., Chou, C.J., Sole, J., Nichols, A., Ross, J.S., Tartaglia, L.A.*, et al.* (2003). Chronic inflammation in fat plays a crucial role in the development of obesity-related insulin resistance. J Clin Invest *112*, 1821-1830.

Yamamoto, M., Yanagisawa, R., Motomura, E., Nakamura, M., Sakamoto, M., Takeya, M., and Eto, K. (2013). Increased methylmercury toxicity related to obesity in diabetic KK-Ay mice. J Appl Toxicol.

Yan, L., Combs, G.F., Jr., DeMars, L.C., and Johnson, L.K. (2011). Effects of the physical form of the diet on food intake, growth, and body composition changes in mice. J Am Assoc Lab Anim Sci *50*, 488-494.

Yasutake, A., Nakano, A., Miyamoto, K., and Eto, K. (1997). Chronic effects of methylmercury in rats. I. Biochemical aspects. Tohoku J Exp Med *182*, 185-196.

Yu, C., Chen, Y., Cline, G.W., Zhang, D., Zong, H., Wang, Y., Bergeron, R., Kim, J.K., Cushman, S.W., Cooney, G.J.*, et al.* (2002). Mechanism by which fatty acids inhibit insulin activation of insulin receptor substrate-1 (IRS-1)-associated phosphatidylinositol 3-kinase activity in muscle. J Biol Chem *277*, 50230-50236.

Zhou, Y.P., Teng, D., Dralyuk, F., Ostrega, D., Roe, M.W., Philipson, L., and Polonsky, K.S. (1998). Apoptosis in insulin-secreting cells. Evidence for the role of intracellular Ca2+ stores and arachidonic acid metabolism. J Clin Invest *101*, 1623-1632.

I. APPENDIX – DIET COMPOSITION

Table A1. Feed preparation recipe and reported values from the laboratory at NIFES. Units of measurements are presented individually, displaying ingredients (g/kg), contaminant pressure (mg/kg), the energy content (kcal/g) and macronutrient composition (%).

Diet composition							
	Ingredients	Low fat (g/kg)	High fat/ High sugar (g/kg)	HF/HS 0.3 mg/kg (g/kg)	HF/HS 1 mg/kg (g/kg)	HF/HS 3 mg/kg (g/kg)	HF/HS 10 mg/kg (g/kg)
Basemix	Vitamin mix	10	10	10	10	10	10
	Mineral mix	35	35	35	35	35	35
	Cellulose	50	50	50	50	50	50
	Choline Hydrogentartrate	2,5	2,5	2,5	2,5	2,5	2,5
	L-cystine	3	3	3	3	3	3
	T-butylhydrochinon	0,014	0,014	0,014	0,014	0,014	0,014
Individual-Diet	Sucrose (powdered sugar)	90	438	438	438	438	438
	Dextrin	540	12	12	12	12	12
	Casein	200	200	200	200	200	200
	Corn oil	70	250	250	250	250	250
Total amount (kg)		1000,5	1000,5	1000,5	1000,5	1000,5	1000,5
Contaminant MeHg-cys (mg/kg)*		-	-	0,3*	1*	3*	10*
Kcal/g		3,95	4,85	4,85	4,85	4,85	4,85
	**Carohydrates (%)*	*630*	*450*	*450*	*450*	*450*	*450*
*Reported value**	*Protein (%)*	*190*	*180*	*175*	*180*	*175*	*180*
	Fat (%)	*63*	*240*	*240*	*240*	*240*	*240*
	MeHg-Cys (mg/kg)	*-*	*-*	*0,54*	*0,83*	*2,4*	*8,29*
	Kcal/g	*4,45*	*4,50*	*5,30*	*5,30*	*5,25*	*5,20*

Table A2. List of suppliers for dietary components

Ingredients	**Supplier**
Vitamin mix	Special Diets Services
Mineral mix	Special Diets Services
Cellulose	Apotekproduksjon A/S
Choline Hydrogentartrate	Merck
L-cystine	Sigma Life Science
T-butylhydrochinon	Aldrich
Sucrose (powdered sugar)	Eldorado
Dextrin	Hoff
Casein	Sigma Life Science
Corn oil	Eldorado
MeHg-cystein	
L-cystein hydrochloride monohydrate MW (175,6 g/mol)	Sigma Life Science
Rectified alcohol	Arcus kjemi, Norway
Methylmercury solution	Sigma Life Science
RNase free ddH2O	MiliQ Millipore, USA

Table A3. Methylmercury concentrations (ml) and ethanol/water solutions (ml) for each experimental diet.

Diet	50:50 Ethanol/Water solution (ml)	MeHg-Cys solution (ml)
0 mg/kg (x2)	60	
0,3 mg/kg	58,3	1,68
1 mg/kg	54	6
3 mg/kg	43,2	16,8
10 mg/kg	4,2	55,8

II. APPENDIX - ELISA

Table A4. Insulin Mouse ELISA kit.

Product	Supplier
Insulin Mouse Ultrasensitive ELISA Kit	DRG Instruments GmbH, Germany
Coated plate	DRG Instruments GmbH, Germany
Calibrator 0 (1 vial)	DRG Instruments GmbH, Germany
Calibrator 1,2,3,4,5 (5 vials)	DRG Instruments GmbH, Germany
Enzyme Conjugate 11X (1 vial)	DRG Instruments GmbH, Germany
Enzyme Conjugate buffer (1 vial)	DRG Instruments GmbH, Germany
Wash buffer (1 bottle)	DRG Instruments GmbH, Germany
Substrate TMB (1 bottle)	DRG Instruments GmbH, Germany
Stop solution (1 vial)	DRG Instruments GmbH, Germany

III. APPENDIX – QUANTITATIVE POLYMERASE CHAIN REACTION

Table A5. Reagents and chemicals used during homogenization and RNA extraction

Product	**Supplier**
Rnase ZAP	Sigma, USA
Trizol	Invitrogen, Norge
Chloroform	VWR international, USA
Isopropanol	Arcus kjemi, Norway
Ethanol	Arcus kjemi, Norway
DEPC	Sigma, USA
RNase free ddH2O	MiliQ Biocel apparatus, Nifes

Table A6. Reagents and chemicals used during RNA precipitation.

Reagent	Supplier
3 M NaAc pH 5.2	
0.1% DEPC H20	Sigma Life Science
Ethanol	Arcus kjemi, Norway
ddH20	MilliQ Biocel, USA

Table A7. Reagents and chemicals used when assessing RNA quality (Agilent 2100 Bio analyzer)

Product	Supplier
Rnase zap	Sigma, USA
Rnase free ddH2O	MilliQ Biocel Apparatus, USA
RNA 6000 Nano LabChip Kit	Agilent Technologies, USA
RNA 6000 Nano Ladder	Ambion, USA

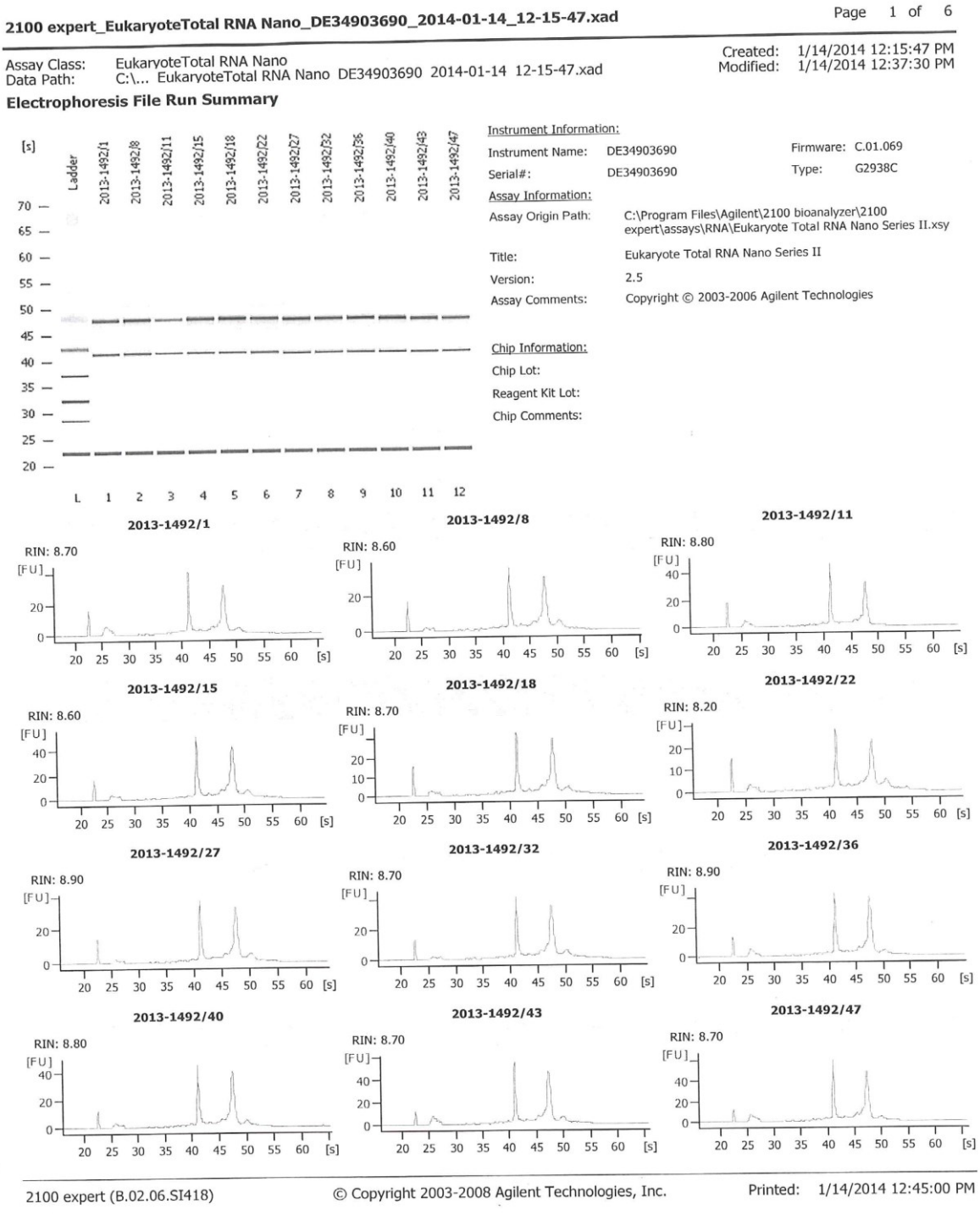

Figure A1. RIN-numbers of 12 random samples obtained from bioanalyser.

Table A8. Reagents and chemicals used during reverse transcriptase reaction.

Reagents	Volume per sample (µl)	Supplier
ddH20	2,8	MiliQ Biocel, USA
Forward primer (50µM)	0,1	Invitrogen, UK
Backward primer (50µM)	0,1	Invitrogen, UK
SYBR GREEN mastermix	5	Roche, Norway

Table A9. List of primers used in Real-time PCR.

Gene	Forward primer (5' primer)	Reverse primer (3'
Tbp	ACCCTTCACCAATGACTCCTATG	ATGATGACTGCAGCAAATCGC
Cd68	CTTCCCACAGGCAGCACAG	AATGATGAGAGGCAGCAAGAGG
F4/80	CTTTGGCTATGGGCTTCCAGTC	GCAAGGAGGACAGAGTTTATCGTG
Fas	CTTCGCCAACTCTACCATGG	TTCCACACCCATGAGCGAGT
Ccl1	GTGTTGGCTCAGCCAGATGC	GCTTGGTGACAAAAACTA
Pck1	CCACACCATTGCAATTATGC	CATATTTCTTCAGCTTGCGG
Ppargc1a	CATTTGATGCACTGACAGATGGA	CCGTCAGGCATGGAGGAA
Ppara	CGTTTGTGGCTGGTCAAGTT	AGAGAGGACAGATGGGGCTC
Pparg	ACAGCAAATCTCTGTTTTATGC	TGCTGGAGAAATCAACTGTGG
Srebf1	GGA GCC ATG GAT TGC ACA TT	GCT TCC AGA GAG GAG CCC AG
Tnf α	CCCTCACACTCAGATCATCTT	GCTACGACGTGGGCTACAG
Pai	AGCGGGACCTAGAGCTGGTC	CCAGTAAGTCACTGATCATACCTTTGGT
Scd 1	GATGTTCCAGAGGAGGTACTACAAGC	ATGAAGCACATCAGCAGGAGG
Acc1	TGCTGCCCCATCCCCGGG	TCGAACTCTCACTGACACG
Foxo1	TTTCTAAGTGGCCTGCGAGTC	CCCATCTCCCAGGTCATCC
Gl6	CTT CAA GTG GAT TCT GTT TGG	AGA TGA CGT TCA AAC ACC GG

IV. APPENDIX - HISTOLOGY

Table A10. Reagents used during the process of staining

Product	Supplier
4 % formaldehyd	Merck, Germany
NaH2PO4 x H2O	Merck, Germany
Na2HPO4 x H2O	Merck, Germany
Zinc Formalin Fixative	Sigma, USA
Ethanol	Arcus, Norway
Rectified Alcohol	Arcus, Norway
Xylene	VWR International, USA
Paraffin	Histovax, OneMed
Hematoxylin	EMS
Eosin	Sigma, USA
Hoecsht 33258	Merck, Germany
Entellan mounting medium (Xylene-based)	Merck, Germany
Fluorescent mounting medium	Sigma, USA

Table A11. Tissue dehydration schedule.

Reagent	Time
75 % Alcohol	45 min
95 % Alcohol	2 x 45min
100 % Alcohol	3 x 45 min
Xylene	2 x 45 min
Paraffin	overnight
Paraffin	2 x 15 min

Table A12. Time schedule used in hematoxilin/eosin staining of pancreatic tissue.

Reagent	Time
Xylene	2 x 10 min
100 % EtOH	2 x 10 min
95 % EtOH	2 x 5 min
75 % EtOH	5 min
50 % EtOH	5 min
ddH2O	5 min
Hematoxylin	30 sec
H2O	4 min
Eosin	5 sec
H2O	4 min
ddH2O	1 min
50 % EtOH	2 min
75 % EtOH	2 min
95 % EtOH	2 x 2 min
100 % EtOH	2 x 5 min
Xylene	2 x 5 min

Table A13. Time schedule used in Hoechst 33258 staining of pancreatic tissue.

Reagent	**Time**
Xylene	2 x 10 min
100 % EtOH	2 x 10 min
95 % EtOH	2 x 5 min
80 % EtOH	5 min
70% EtOH	5 min
50 % EtOH	5 min
ddH2O	5 min
Hoechst 33258	10 min
H2O	10 min

V. APPENDIX – HEPATIC GENE EXPRESSION

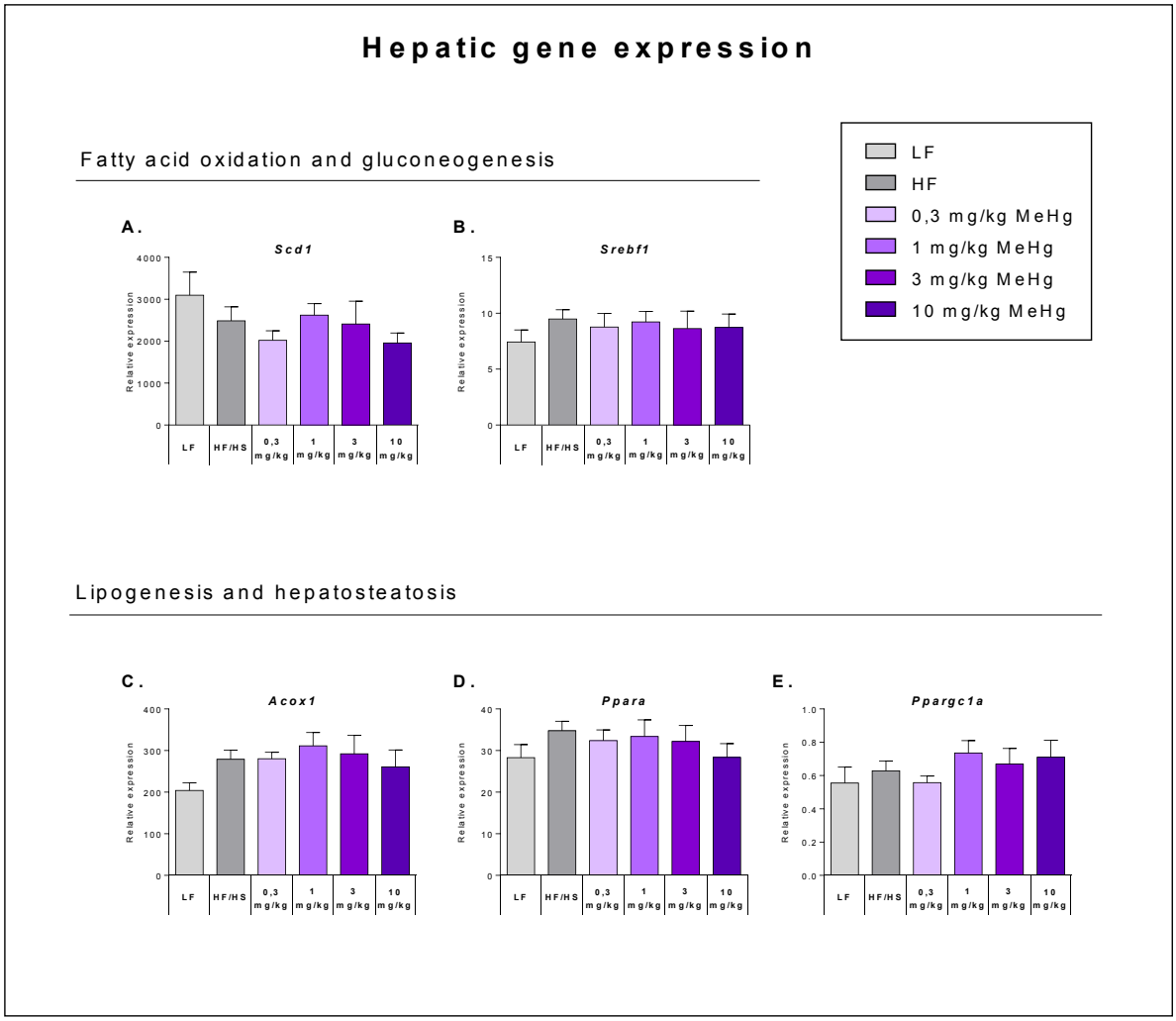

Figure A2. The effect of methylmercury on expression of genes involved in metabolic regulation.

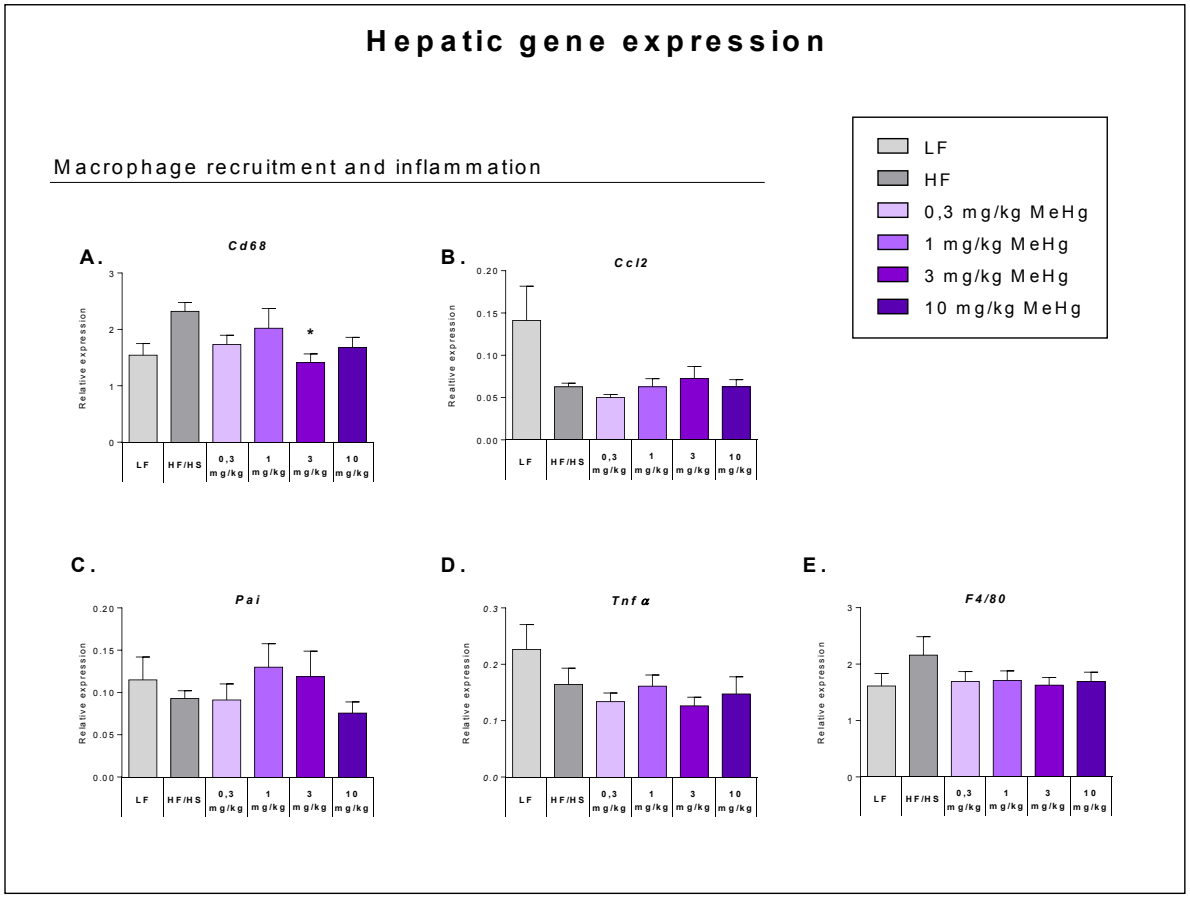

Figure A3. The effect of methylmercury on expression of inflammation and macrophage infiltration markers.

VI. APPENDIX – ORGAN MASS

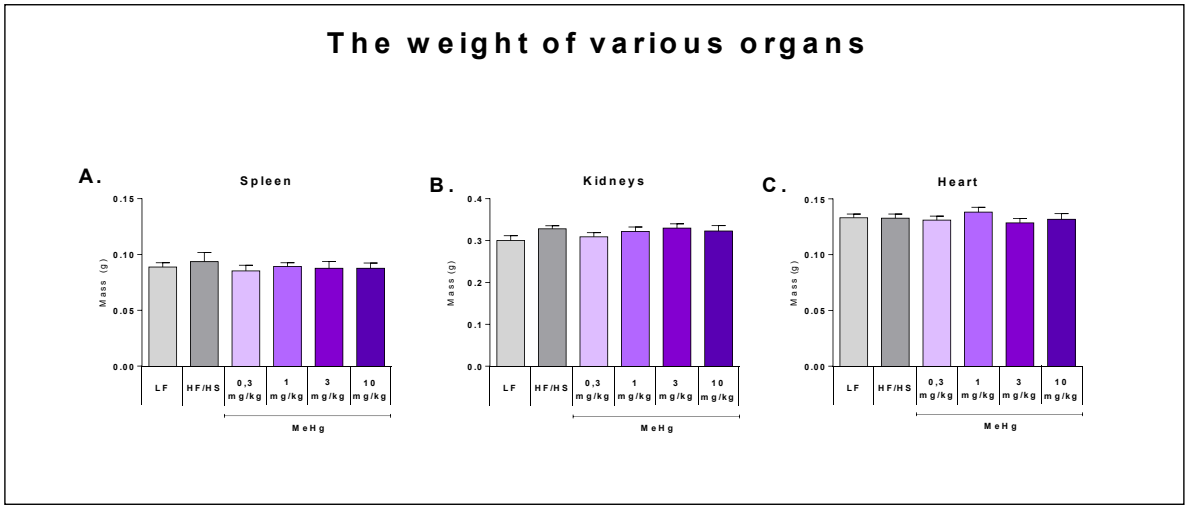

Figure A4. Organ masses (g).

VII. APPENDIX – HISTOLOGICAL IMAGES

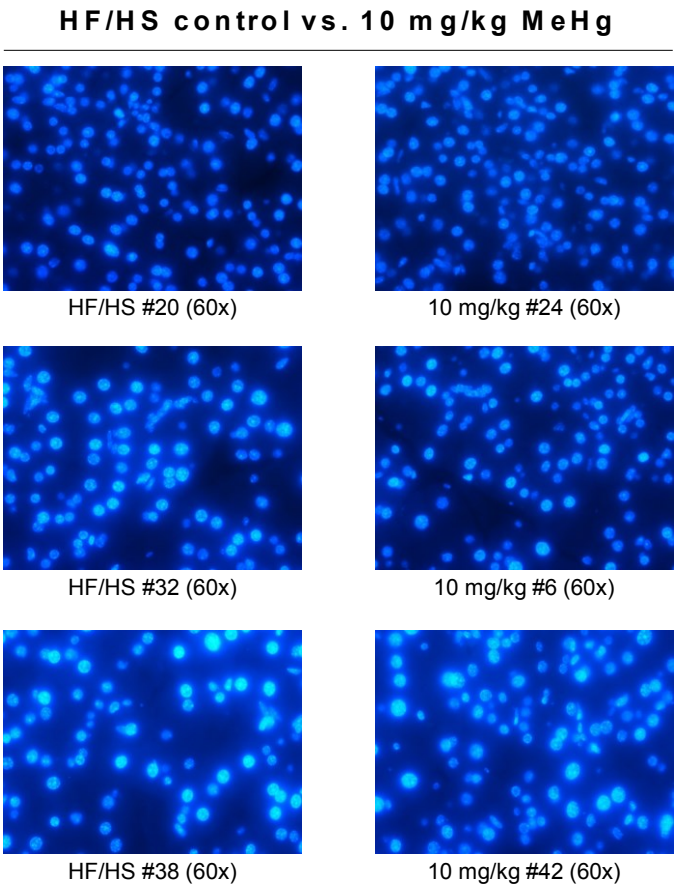

Figure A5. Histopathology examinations of pancreatic sections.

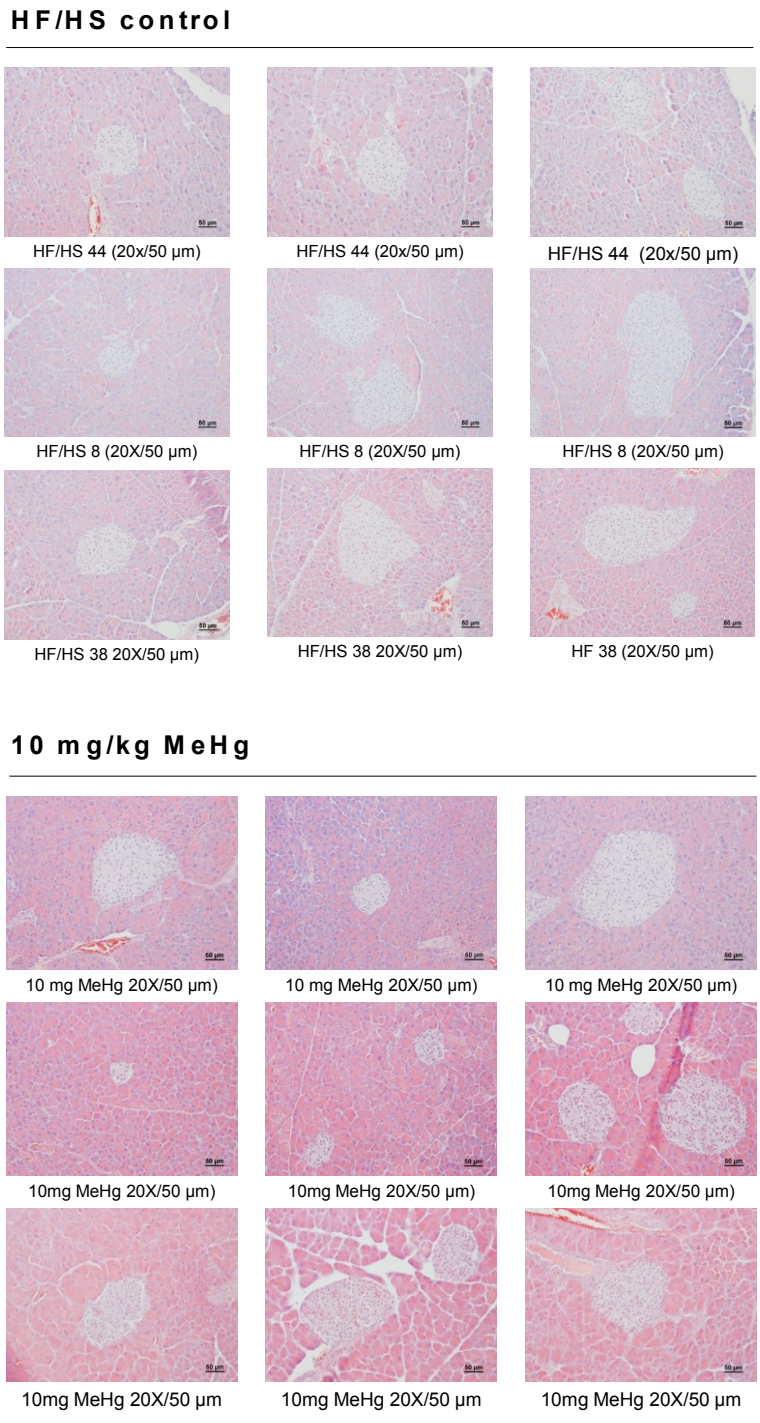

Figure A6. Histopathological assessments of pancreatic mouse tissue.